Naval Environmental Prediction Research Facility
Monterey, CA 93943-5006

Technical Report TR 87-05 December 1987

THE SURFACE EVAPORATIVE DUCT HEIGHT PRODUCT: AN EVALUATION

William T. Thompson
Naval Environmental Prediction Research Facility

UNCLASSIFIED

SECURITY CLASSIFICATION OF THIS PAGE

REPORT DOCUMENTATION PAGE

1a REPORT SECURITY CLASSIFICATION: UNCLASSIFIED	1b RESTRICTIVE MARKINGS
2a SECURITY CLASSIFICATION AUTHORITY	3 DISTRIBUTION / AVAILABILITY OF REPORT: Approved for public release; distribution is unlimited
2b DECLASSIFICATION / DOWNGRADING SCHEDULE	
4 PERFORMING ORGANIZATION REPORT NUMBER(S): TR 87-05	5. MONITORING ORGANIZATION REPORT NUMBER(S)
6a. NAME OF PERFORMING ORGANIZATION: Naval Environmental Prediction Research Facility; 6b OFFICE SYMBOL (If applicable)	7a. NAME OF MONITORING ORGANIZATION
6c. ADDRESS (City, State, and ZIP Code): Monterey, CA 93943-5006	7b. ADDRESS (City, State, and ZIP Code)
8a. NAME OF FUNDING / SPONSORING ORGANIZATION: Space and Naval Warfare Systems Command; 8b. OFFICE SYMBOL (If applicable): PMW-141	9. PROCUREMENT INSTRUMENT IDENTIFICATION NUMBER
8c. ADDRESS (City, State, and ZIP Code): Department of the Navy, Washington, DC 20363-5100	10 SOURCE OF FUNDING NUMBERS: PROGRAM ELEMENT NO. 63207; PROJECT NO. W0513; TASK NO.; WORK UNIT ACCESSION NO. DN656770

11 TITLE (Include Security Classification): The Surface Evaporative Duct Height Product: An Evaluation (U)

12. PERSONAL AUTHOR(S): Thompson, William T.

13a. TYPE OF REPORT	13b. TIME COVERED	14. DATE OF REPORT (Year, Month, Day)	15. PAGE COUNT
Final	FROM 10/1/86 TO 9/30/87	1987, December	55

16 SUPPLEMENTARY NOTATION

17 COSATI CODES		
FIELD	GROUP	SUB-GROUP
04	01	

18. SUBJECT TERMS (Continue on reverse if necessary and identify by block number)
Microwave refractivity, Atmospheric stability
Surface evaporative duct, Similarity theory
Atmospheric boundary layer, GSCLI, NOGAPS

19 ABSTRACT (Continue on reverse if necessary and identify by block number)

The global surface evaporative duct (SED) height field is produced operationally at the Fleet Numerical Oceanography Center (FNOC) by the global surface contact layer interface (GSCLI) model. An evaluation of the quality of the product and an analysis of the GSCLI SED algorithm were conducted. Results indicate that there is a considerable geographical bias in the quality of the product. The expression used to compute duct height contains several simplifications and produces unrealistic values for duct height under certain conditions. It is recommended that a different expression be adopted for duct height determination when the surface layer is stable.

20 DISTRIBUTION / AVAILABILITY OF ABSTRACT: ☒ UNCLASSIFIED/UNLIMITED ☐ SAME AS RPT ☐ DTIC USERS	21 ABSTRACT SECURITY CLASSIFICATION: UNCLASSIFIED
22a NAME OF RESPONSIBLE INDIVIDUAL: Thompson, William T.	22b TELEPHONE (Include Area Code): (408) 647-4716; 22c OFFICE SYMBOL: NEPRF WU 6.3-1

DD FORM 1473, 84 MAR 83 APR edition may be used until exhausted. All other editions are obsolete.

SECURITY CLASSIFICATION OF THIS PAGE

UNCLASSIFIED

CONTENTS

1. INTRODUCTION

This report evaluates the surface evaporative duct height field produced by the global surface contact layer interface model at the Fleet Numerical Oceanography Center (FNOC). This evaluation is intended to inform users of the product's ability to provide a representative analyses and forecast(s) of global surface ducting conditions.

Analysis and forecast fields from the Navy Operational Global Atmospheric Prediction System (NOGAPS) are required as input for the creation of the surface evaporative duct height field. This evaluation was conducted prior to the implementation of NOGAPS 3.0 by the FLENUMOCEANCEN in January 1988. Thus, some of the conclusions discussed below may no longer be valid. An analysis similar to the one described below could be performed in order to assess the impact of the new global prediction system.

A surface evaporative duct is said to exist when a rapid decrease in specific humidity q near the surface results in a decrease in the modified index of refraction M with altitude (Richter and Hitney, 1979). The relationship between M and q is

$$N = 77.6\ P/T + 3.73 \times 10^6\ e/T^2$$

$$M = N + z/a$$

where

$$q = 0.622e/(P - 0.378e)$$

and where P is the pressure (mb), T is the absolute temperature (K), e is the vapor pressure (mb), z is the altitude (m), and a is the radius of the earth.

When $dM/dz < 0$, microwave energy may be trapped near the surface and radar return strength may be enhanced. Microwave rays within the duct, traveling in directions near grazing incidence with the duct boundaries, may be unable to penetrate the duct and may be reflected by the duct boundary and the sea surface. Thus, such rays will be able to travel long distances downrange with minimal loss in signal strength. The critical incidence angle for trapping depends on frequency, duct height, and duct strength (Ko et al., 1983). Low frequencies, in general, do not have as large a variation in extended range with varying duct heights as higher frequencies, and higher frequencies do not require as large a duct thickness for the same range enhancement as lower frequencies (Polios and Hitney, 1979). The height of the duct is where the lowest inflection appears in the M profile and the strength of the duct is the magnitude of dM/dz (Ko et al., 1983). Sea clutter is also enhanced in ducting situations.

Many circumstances which would lead to large gradients in q near the surface of the ocean can be envisioned. In fact, surface evaporative ducting is nearly always present over almost all oceans (Richter and Hitney, 1979).

The existence of a surface evaporative duct has many serious operational implications. One of the most serious and obvious implications is that the extended range of the radar will allow distant hostile units to detect the radar (and to be detected by the radar). Thus, the existence of a surface evaporative duct is an important component of the decision on whether or not to

radiate. Another consequence of the duct is that a radar "hole" will exist between the top of the duct and the base of the lobes unaffected by the duct (see Figure 1). Hostile aircraft or missiles will thus be able to approach the radar undetected. Conversely, knowledge of the refractivity profile in the vicinity of enemy radars can be turned to tactical advantage.

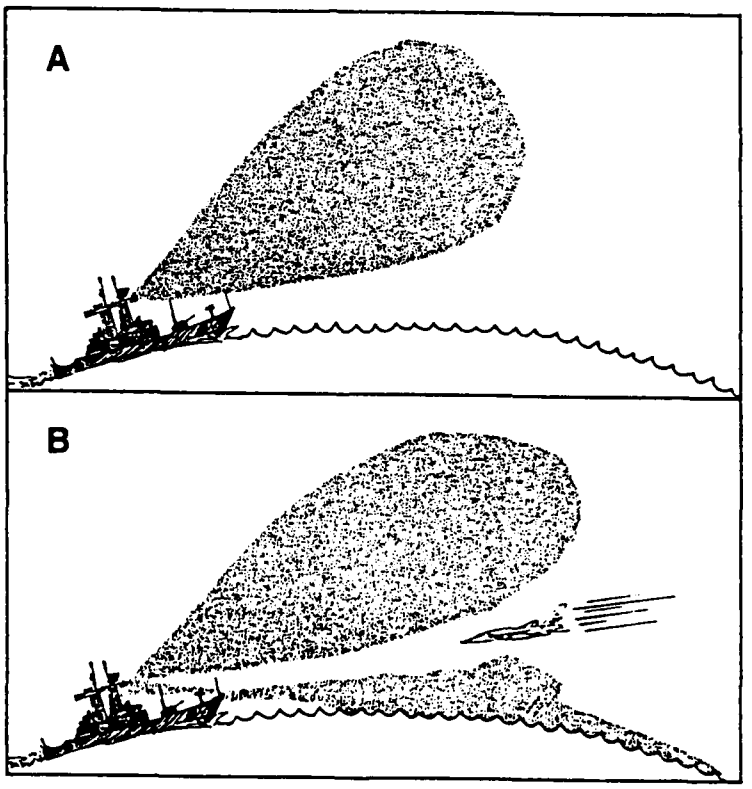

Figure 1. Schematic of shipboard radar coverage under normal atmospheric conditions, no ducting, A; and changes in the presence of an evaporation duct, B. Under ducting conditions an aircraft in the radar "hole" can not be seen by the ship's radar, as indicated in B.

Enhanced sea clutter may also pose a threat. Sea clutter may have a cross-section larger than a low-flying aircraft or missile, thereby hiding it from the radar. Also, automated tracking systems can be saturated and disabled by elements of sea clutter. (Snyder, 1979). An unusual amount of sea clutter, however, will provide the operator with evidence of ducting conditions. This may be the only indication of ducting if the refractivity profile is not known.

There are several sources of operational information on refractivity. The easiest to use is the refractive effects guidebook (REG) in which synoptic typing is used to associate certain refractivity profiles with climatological patterns. Surface evaporative ducts, however, are beyond the scope of the Refractive Effects Guidebook (REG) published by NEPRF (Rosenthal, 1976). Another source of information is the Integrated Refractive Effects Prediction System (IREPS), which requires as input a radiosonde sounding. When an elevated trapping layer overlies a surface evaporative duct, the behavior of the radar will be dramatically effected (Sketchly, 1979). In such a situation, however, IREPS will assume that the surface duct is the dominant feature (Paulus and Hitney, 1979). Finally, the sea clutter algorithms in IREPS are more consistent with ducts based at the surface formed by elevated refractive layers [i.e., a duct in which the elevated minimum in the M profile is smaller than the surface value] (Snyder, 1979). Although IREPS is capable of diagnosing the thickness of the surface evaporative duct, the only product specifically designed for the prediction of surface evaporative ducts is the surface evaporative duct

height field produced at the FNOC by the Global Surface Contact Layer Interface (GSCLI) model.

2. GLOBAL SURFACE CONTACT LAYER INTERFACE MODEL

The GSCLI model is a generalized similarity theory model for the entire planetary boundary layer (PBL) in which three nondimensional parameters are assumed to completely determine the momentum and mass fields within the PBL. The first two parameters are the surface Rossby number Ro and the temperature stratification parameter S:

$$Ro = G(fz_o)^{-1}$$

$$S = g\Delta\theta_v \, (\theta_v f G)^{-1}$$

where

$$\Delta\theta_v = \theta_{v_x} - \theta_{v_o}$$

$$\Delta q = qx - q_o$$

and where G is the 500 m gradient wind, f is the Coriolis parameter, z_o is the roughness length (which is a function of wind speed), and g is the acceleration due to gravity. The subscript "x" refers to the top of the surface layer at h=BG/f (B is a constant) while the subscript "o" refers to the surface. Ro and S determine the barotropic PBL. The third parameter μ introduces baroclinicity:

$$\mu = H'/L$$

where

$$H' = ku_*(f)^{-1}$$

and

$$L = \frac{\theta_v \, u_*^3}{kg \, (u_*\theta_* + 0.609 \, u_* q_*)}$$

and where k is von Karman's constant. The scale velocity u_*, scale virtual potential temperature θ_*, and scale moisture q_* are qiven by

$$u_* = C_D G$$

$$\theta_* = u_*^2 \, \theta_v (k^2 g L)^{-1}$$

$$q_* = C_p \theta_v \, (\Lambda C_p \, \theta_v / \Lambda \Delta q)$$

where C_D is the drag coefficient (which is a function of z/L), C_p is the specific heat of air at constant pressure, and Λ is the latent heat of vaporization. L is the Monin-Obukhov length scale which is a ratio of mechanical to bouyant turbulent kinetic energy production. Ro, S, and μ are determined from output from the Navy Operational Global Atmospheric Prediction System (NOGAPS). Note that the GSCLI is purely a diagnostic system; forecast fields from the GSCLI are generated by using NOGAPS forecast fields for determination of Ro, S, and μ. Within the surface layer, the scaling quantities are related to the mean gradients by

$$\frac{du}{dz} = \frac{u_*}{kz} \, \phi \left(\frac{z}{L}\right)$$

$$\frac{d\theta}{dz} = \frac{\theta_*}{kz} \, \phi \left(\frac{z}{L}\right)$$

$$\frac{dq}{dz} = \frac{q_*}{kz} \, \phi \left(\frac{z}{L}\right)$$

where the diabatic flux-profile function ϕ is given by

$$\phi = 0.74 + 4.7 \left(\frac{z}{L}\right) \qquad \text{stable}$$

$$\phi = 0.74 \left(1-9 \left(\frac{z}{L}\right)\right)^{-1/2} \qquad \text{unstable}$$

and where z is a reference height. Given the scaling quantities q_* and θ_*, an expression for the surface evaporative duct height (derived in Appendix A) can be obtained:

$$\delta = \frac{C\, q_*\, \phi(z/L) - T_*\, \phi(z/L)}{b_2\, T^2/AP + 0.243}$$

where C and A are constants and P is the pressure (mb). b_2 is the critical vertical gradient in N for trapping (= -157 N/Km). δ is produced operationally over all ocean regions at 6 hour intervals from tau 0 to tau 36. The record name is A90. Several related fields are also produced, including A92, the surface N value minus the value at the level where dN/dz = -157 N/Km.

A discussion of surface layer similarity theory as it pertains to near-surface gradients in N appears in Appendix B.

The primary NOGAPS-derived quantities which influence the GSCLI are the low-level pressure gradient and, in the tropics, the PBL wind field (which determines G), the sea-surface temperature field, and the 850 mb temperature field. Thus, the amount of "synoptic" information available to the GSCLI is limited. Determination of atmospheric stability in the GSCLI relies on an extrapolation of the 850 mb temperature to 1000 mb (using the

the 1000-850 mb thickness) and a further extrapolation of the difference between the extrapolated 1000 mb temperature and the sea surface temperature to arrive at the air/sea temperature difference. Stability is critical in determination of δ. It plays a role in determining L, in selecting the appropriate ϕ, and in computing q_* and Θ_*. Several constraints on L, z/L, and θ are required by the formulation of the GSCLI model which limit its generality. A number of ad hoc corrections have also been added in order to improve model performance in certain synoptic situations (e.g., cold air outbreaks).

In light of uncertainties concerning the quality of the model products, a study has been undertaken at the Naval Environmental Prediction Research Facility (NEPRF) in order to evaluate the response of the A90 product to changes in the synoptic pattern. Although the analysis (tau=0) field is subject to the same uncertainties as the forecast fields, the lack of any independent measurements of surface evaporative ducting necessitates verification of the forecast against the analyses.

The analyses presented in Appendices A and B of the expression used for surface evaporative duct height in the GSCLI model clearly demonstrate a serious shortcoming of this expression. Specifically, when the ambient conditions are such that dN/dz never approaches the critical value, the GSCLI model falsely produces reasonable appearing duct heights. When dN/dz is much greater than the critical value, the duct height should be much larger than the value produced by the GSCLI model. When dN/dz is much less than the critical value, no duct exists. Based

on the development in Appendix B, it is strongly recommended that the similarity theory approach for potential refractivity be adopted under stable conditions for the operational surface evaporative duct height product.

3. EVALUATION OF THE SURFACE EVAPORATIVE DUCT HEIGHT PRODUCT

During a period of several months over three seasons, root mean square (RMS) errors were computed for the A90 field each day at both 00Z and 12Z for the 12, 24, and 36 hour forecasts. The error fields were constructed by subtraction of 12, 24, and 36 hour forecasts valid at the analysis time from the analysis field. In addition, the maximum error, location of the maximum error, and higher moments of the error distribution (variance, skewness, and kurtosis) were computed. The RMS errors were relatively insensitive to the length of the forecast; RMS errors in the 12 hour forecast rarely departed very far from the range of 2.9-3.1 m with an increase of only about 15% by 36 hours. Error variance tended to be in the range from 9 to 11 m with an increase of 2-3 m by 36 hours. Maximum errors rarely departed very far from the range of 17-23 m with no discernible trend for increasing length of forecast. No diurnal or seasonal variation was detectable.

3.1 Characteristic Features

Surface evaporative ducts (SED) are primarily the result of large near surface gradients in specific humidity (or vapor pressure). Consequently, one might expect that the most active

surface evaporative ducting regions would be in the tropics where high temperatures and relative humidities lead to high specific humidities. While SED is by no means confined to the tropics, the greatest frequency of occurrence (in the forecast and analyzed A90 field) is in the region from 30 degrees north to 30 degrees south.

Tropical cyclones, in particular, produce a well-defined signature in the SED field. Typically, the tropical cyclone is associated with a local maximum in duct height. High wind speeds promote mechanical mixing which results in a well mixed PBL with large gradients in specific humidity and virtual potential temperature confined to the capping inversion at the PBL top. Large errors in SED forecast fields are associated with tropical cyclones. The tropical cyclone bogus is present in the analysis but not present in the forecast fields. This leads to large differences between analysis and forecast fields in the vicinity of a tropical cyclone.

A characteristic feature associated with the importance of specific humidity is local maxima in duct height due to ocean currents. This is particularly true of warm currents in the winter hemisphere. The relatively warm water promotes large surface moisture fluxes so that the air near the surface is quite moist while the air above is cool and dry. The gulf stream, in particular, is quite evident in the SED fields in January; the maximum SED values coincide with the maximum in the NOGAPS sea surface temperature (SST) field.

A feature conspicuous by its absence is a local maximum in SED height and frequency off the western coasts of continents in the subtropical latitudes of the summer hemisphere. For example, surface ducts are quite commonly observed in the summer in the southern California operating area (Paulus and Hitney, 1979), but do not appear in the analyzed or forecast SED fields.

3.2 Midlatitudes

Midlatitude response of the SED product to storms traversing oceanic areas exhibits a pronounced geographic variability. In the North Atlantic and South Pacific, the product responds well to oceanic extratropical cyclones while it is deficient in the North Pacific and South Atlantic oceans. There is no apparent diurnal difference in forecast quality. Examples of this geographic bias are presented below. Possible causes of the geographical bias are discussed in the conclusion.

Examination of a number of cases reveals several general features. Over the North Atlantic ocean, the forecast ducting response is typically on the south east side of the low pressure area (possibly in the vicinity of the cold front), sometimes appearing as an extension from the duct region associated with the gulf stream. During the Southern Hemisphere winter, ducting is frequently identified in the South Pacific in the area south west of the Chilean coast near Antarctica. This is an area with a high frequency of cyclogenesis. These storms are associated with the advection of extremely cold air off of the Antarctic continent over relatively warm ocean surfaces. Thus, these

storms may activate the model cold air advection parameterization in which the diagnosed air/sea temperature difference is replaced by a prescribed cooling rate based on the geostrophic advection of air/sea temperature difference. Large near surface gradients in temperature contribute to near surface N gradients characteristic of surface evaporative ducts.

Examples of the general features discussed above appear in Figures 2-13. Figures 2-9 show a series of 12 hour sea level pressure (SLP) forecasts with corresponding 12 hour forecasts of SED beginning at 00Z on 29 January and ending at 12Z on 31 January 1987. An intense storm is located in the Gulf of Alaska throughout the period. There is no indication of any ducting anywhere near the Gulf. In Figure 2, note the storm in the North Atlantic near 40 degrees N and 40 degrees W. In Figure 3, note the extension of the duct region near the east coast of North America (near the Gulf Stream) towards the location of the storm. An example of a ducting area on the southeast side of a low in the North Atlantic is shown in Figures 10 and 11 for 00Z on 21 January 1987. In this situation, the duct area appears to be nearly coincident with the area of maximum pressure gradient. Figures 14-16 show a series of forecasts of SED all valid at 00Z on 26 June 1986. The analysis is shown in Figure 12 and the corresponding SLP analysis in Figure 13. This series has several interesting features, including responses to storms near Antarctica. The size and depth of the duct area between the southwest coast of Peru and Antarctica are quite consistent

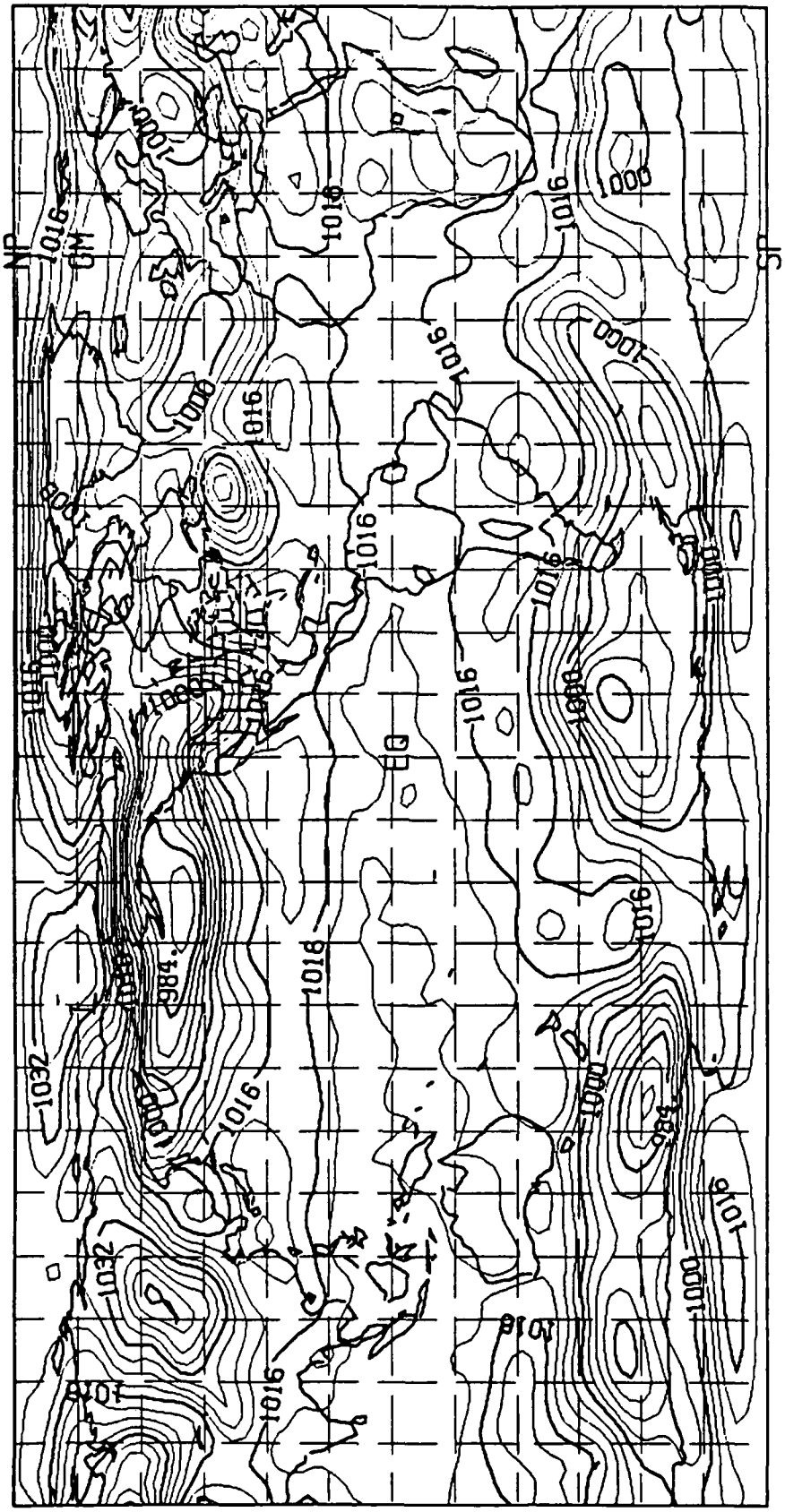

Figure 2. 12 hour forecast of the sea level pressure field valid at 00z on 29 January 1987.

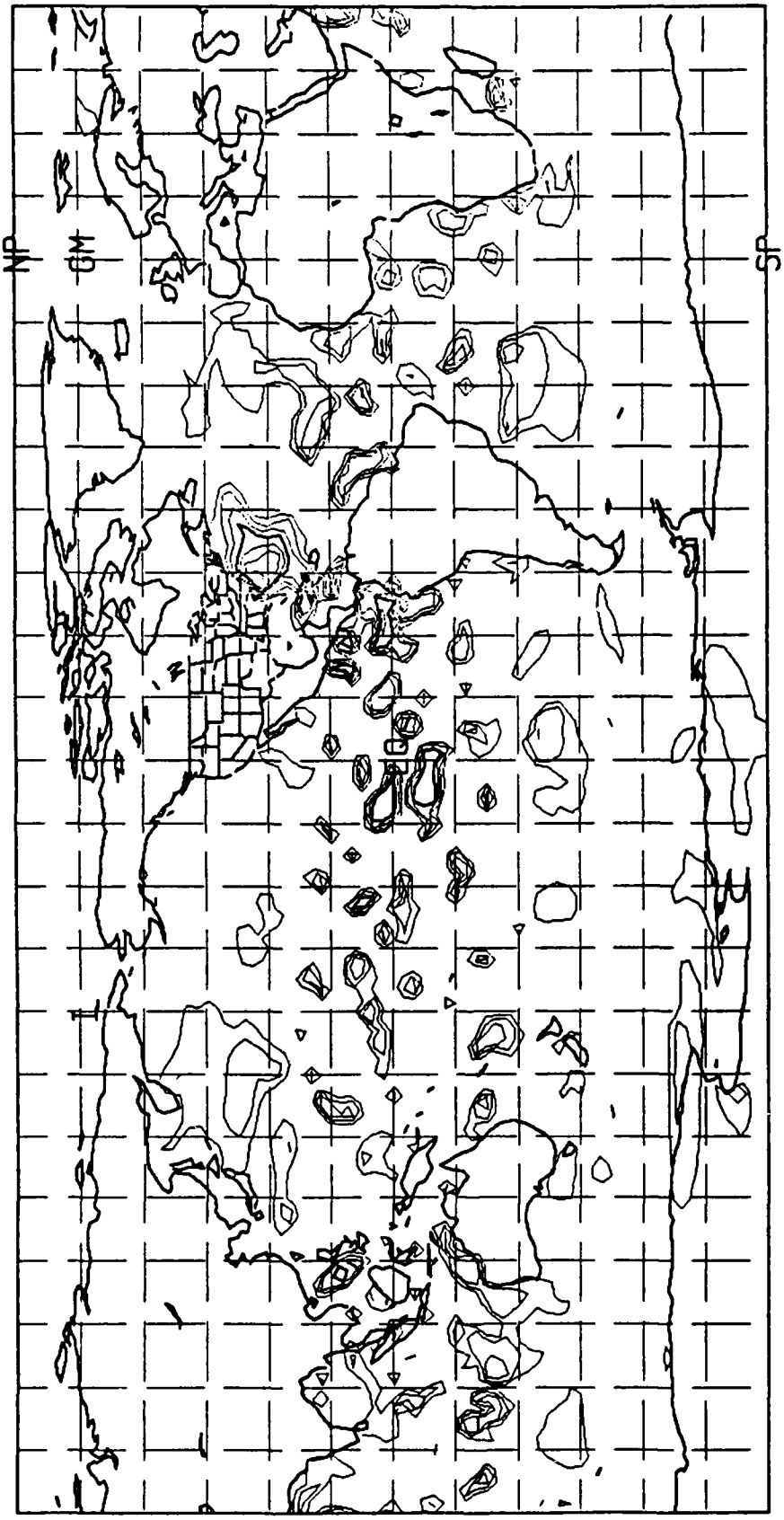

Figure 3. 12 hour forecast of the radar evaporative duct height field valid at 00Z on 29 January 1987.

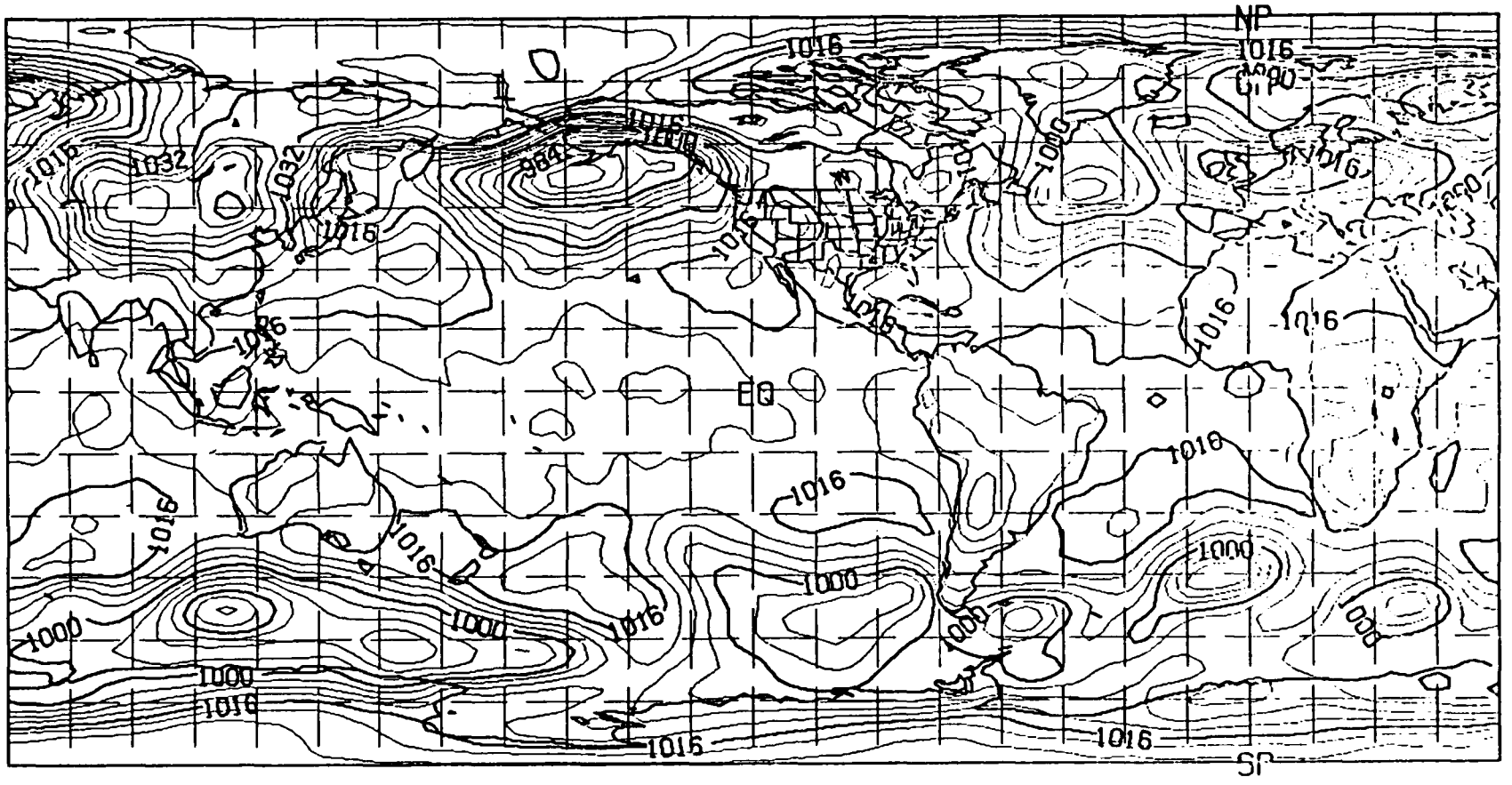

Figure 4. 12 hour forecast of the sea level pressure field valid at 00Z on 30 January 1987.

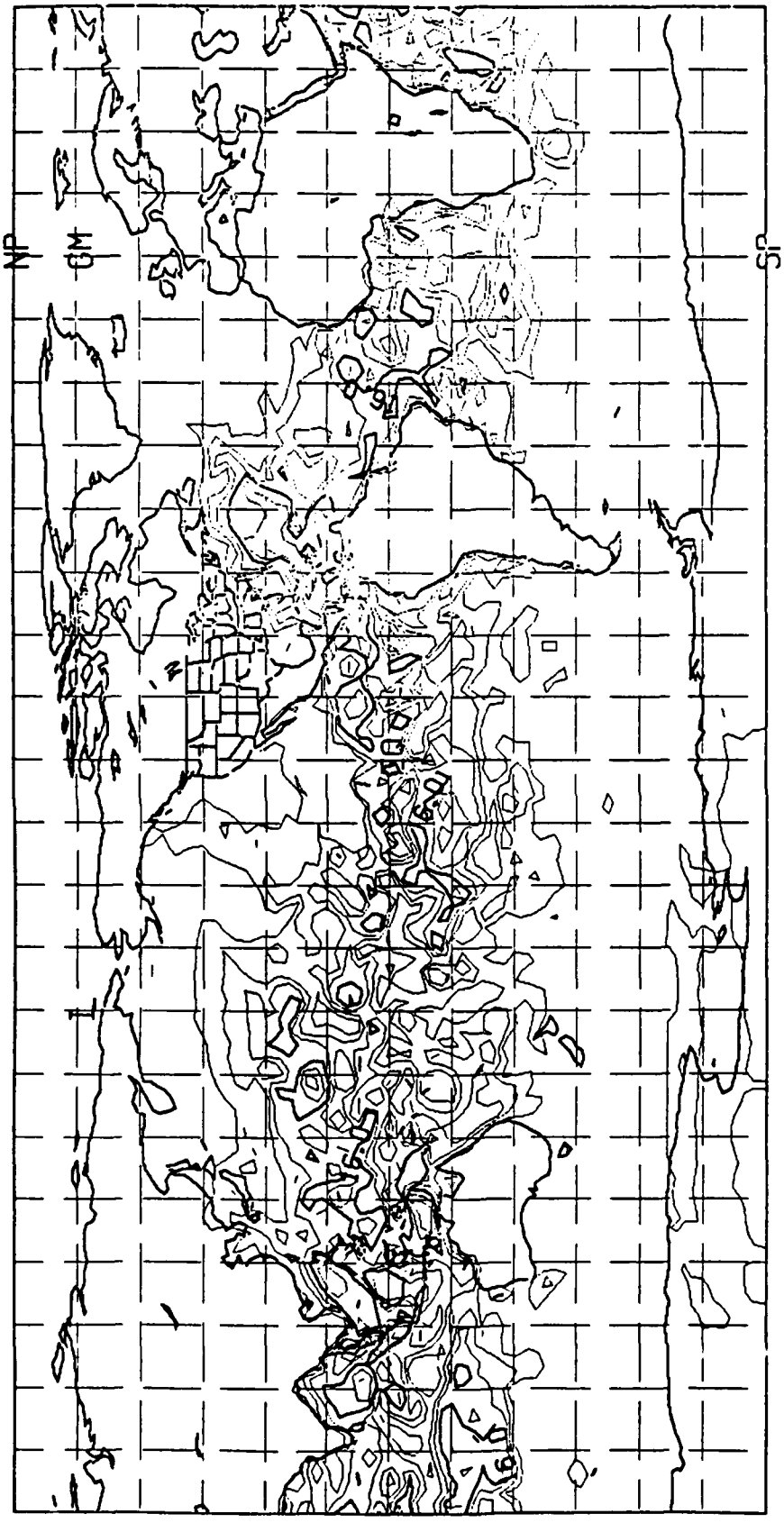

Figure 5. 12 hour forecast of the radar evaporative duct height field valid at 00z on 30 January 1987.

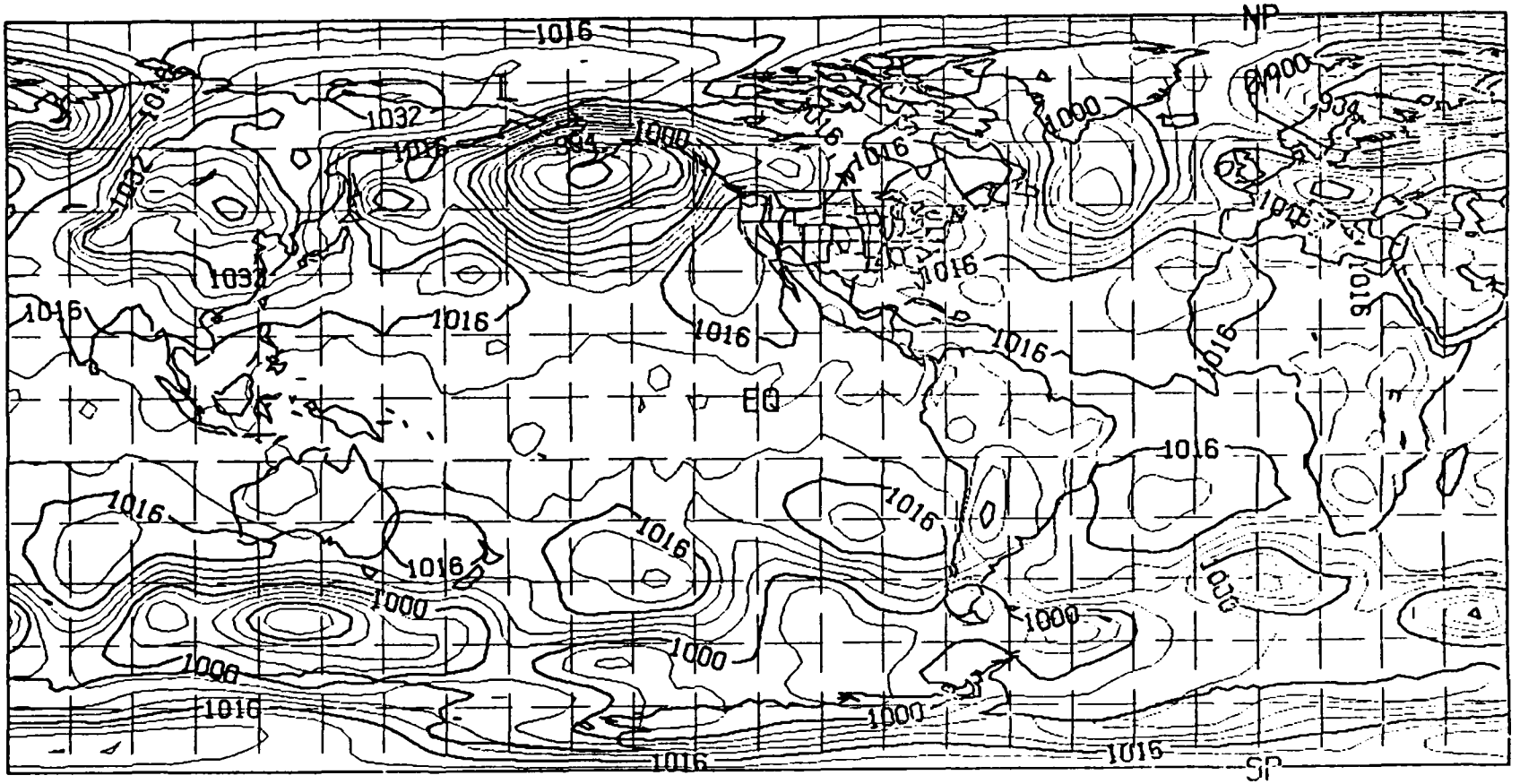

Figure 6. 12 hour forecast of the sea level pressure field valid at 00Z on 31 January 1987.

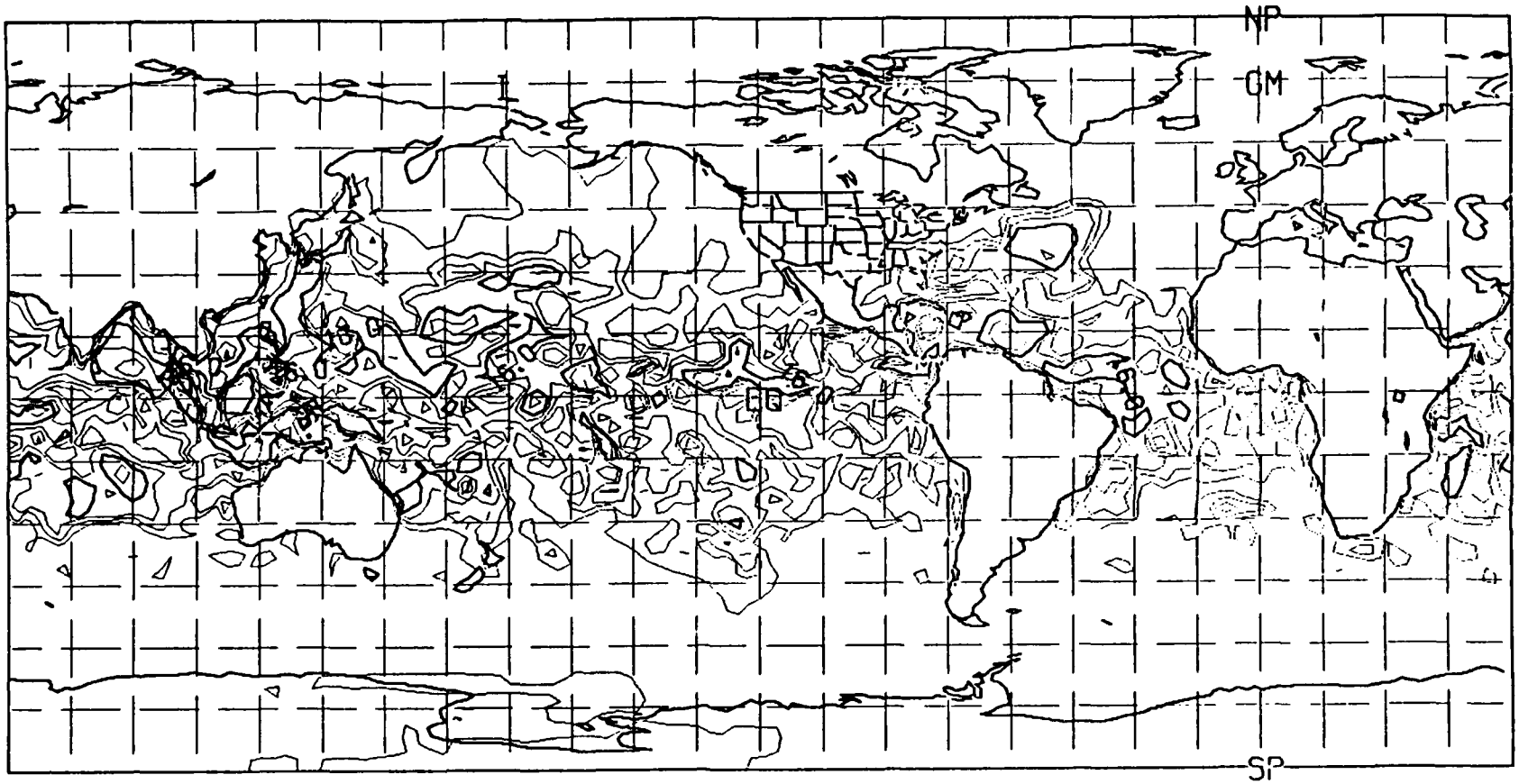

Figure 7. 12 hour forecast of the radar evaporative duct height field valid at 00Z on 31 January 1987.

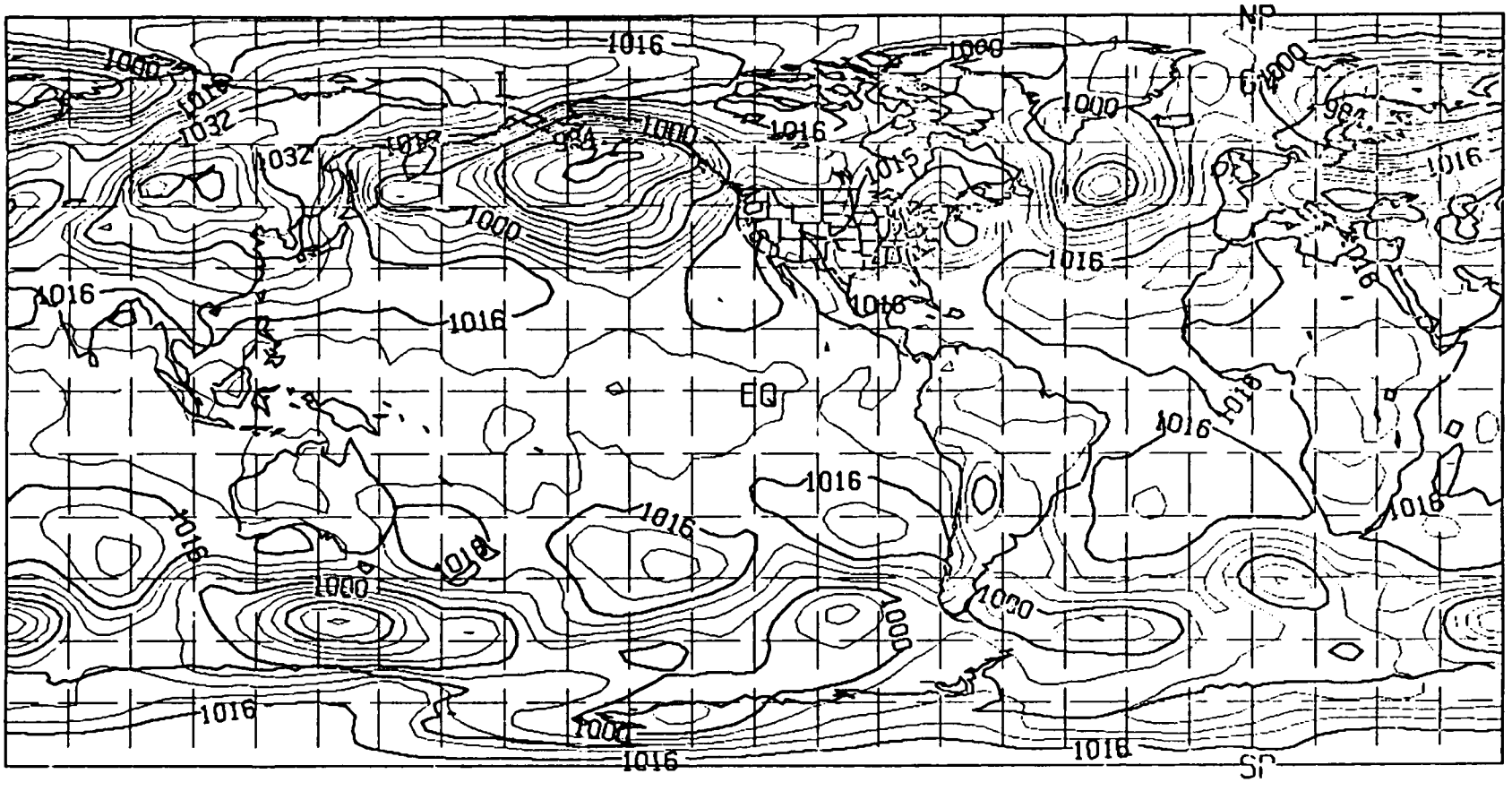

Figure 8. 12 hour forecast of the sea level pressure field valid at 12Z on 31 January 1987.

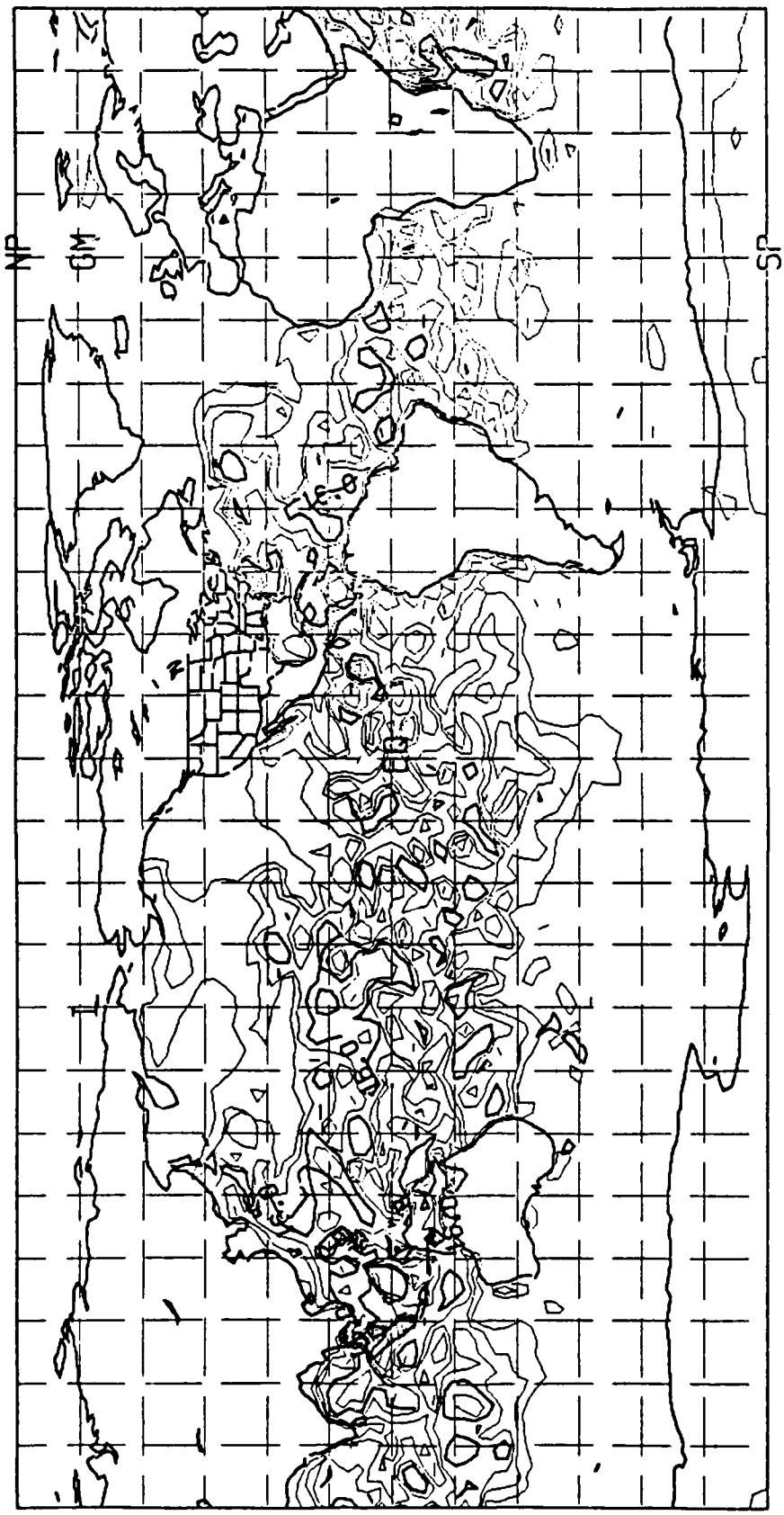

Figure 9. 12 hour forecast of the radar evaporative duct height field valid at 12z on 31 January 1987.

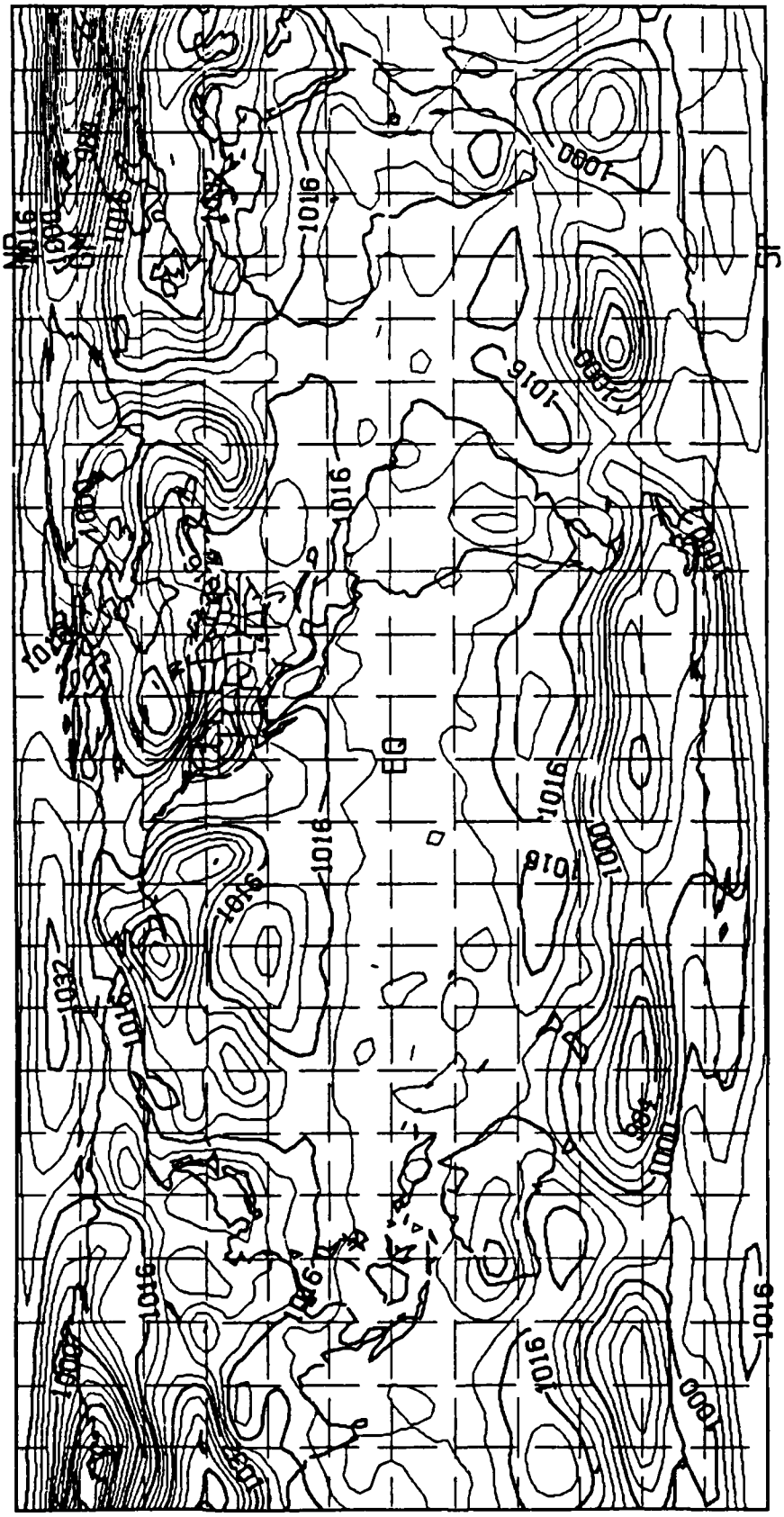

Figure 10. 12 hour forecast of the sea level pressure field valid at 00z on 21 January 1987.

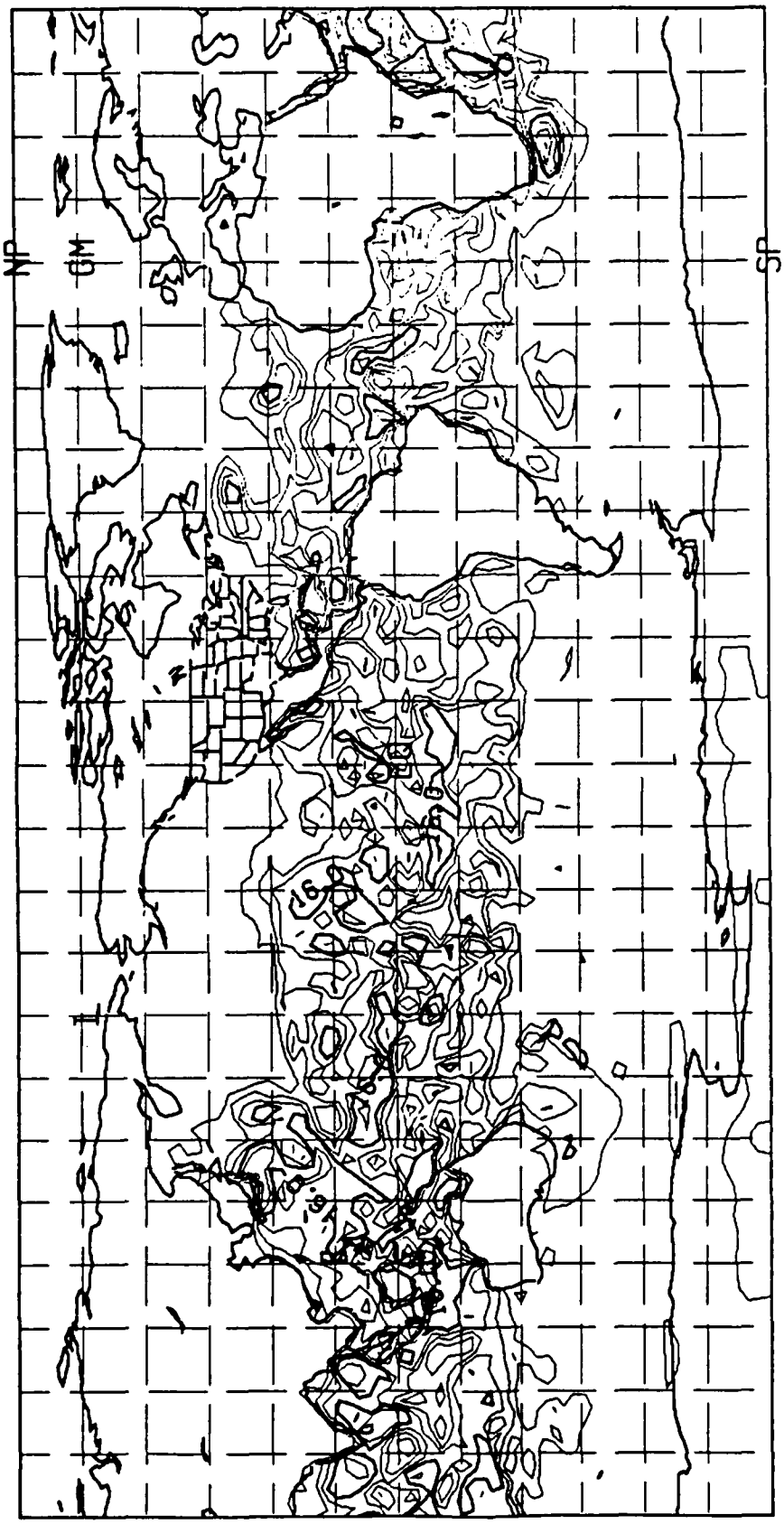

Figure 11. 12 hour forecast of the radar evaporative duct height field valid at 00Z on 21 January 1987.

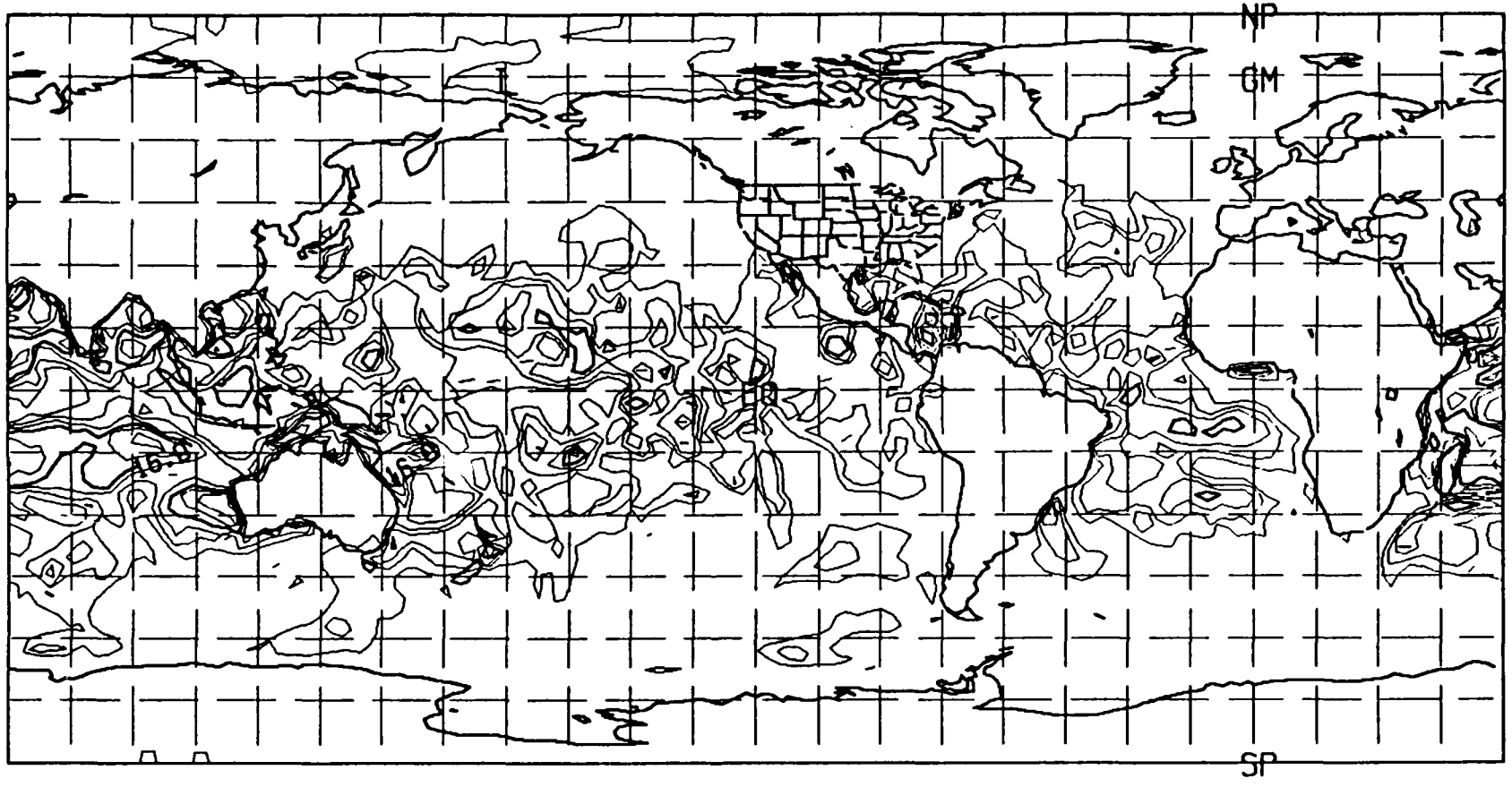

Figure 12. Analysis of the radar evaporative duct height field valid at 00Z on 26 June 1986.

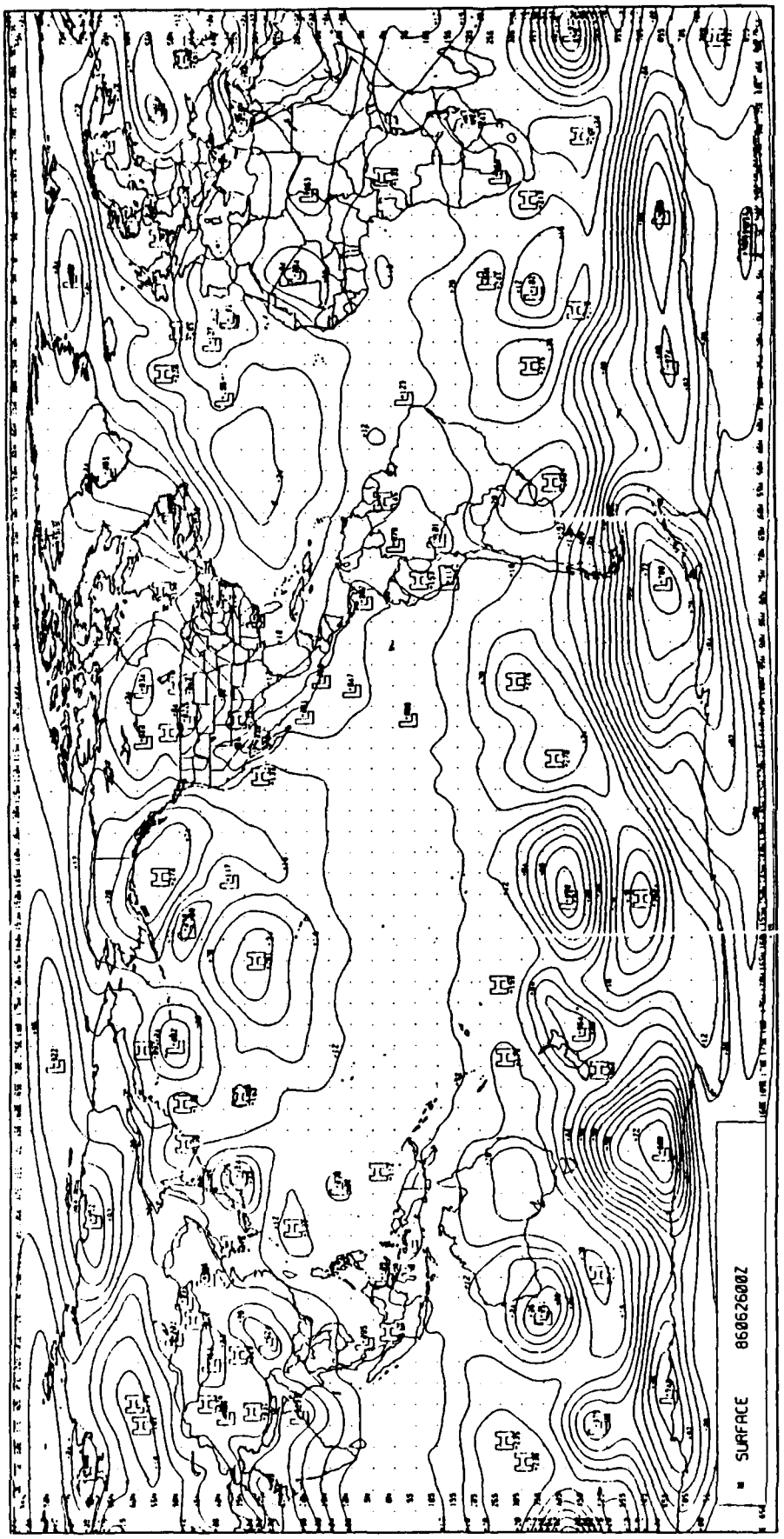

Figure 13. Analysis of the sea level pressure field valid at 00Z on 26 June 1986.

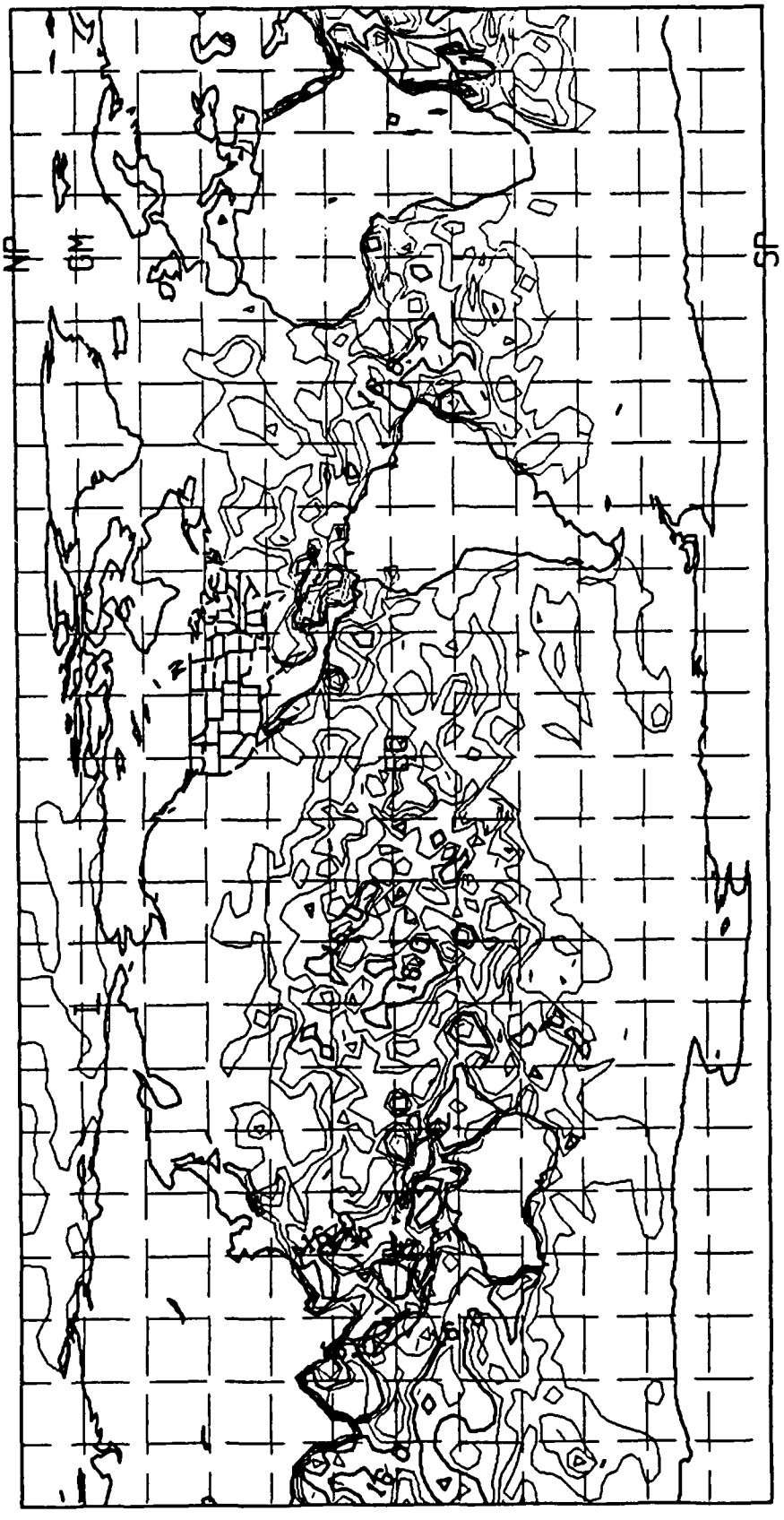

Figure 14. 12 hour forecast of the radar evaporative duct height field valid at 00Z on 26 June 1986.

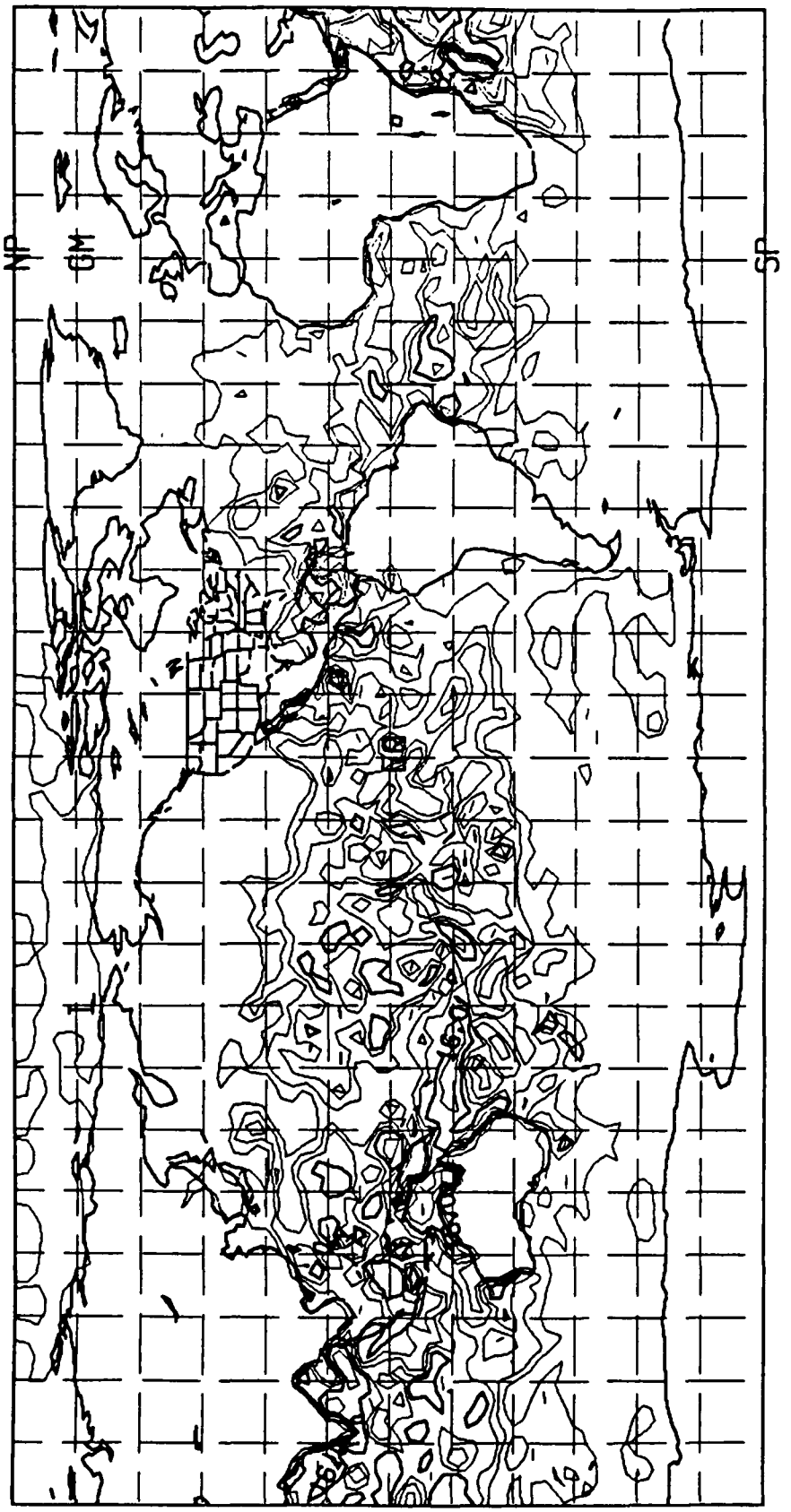

Figure 15. 24 hour forecast of the radar evaporative duct height field valid at 00Z on 26 June 1986.

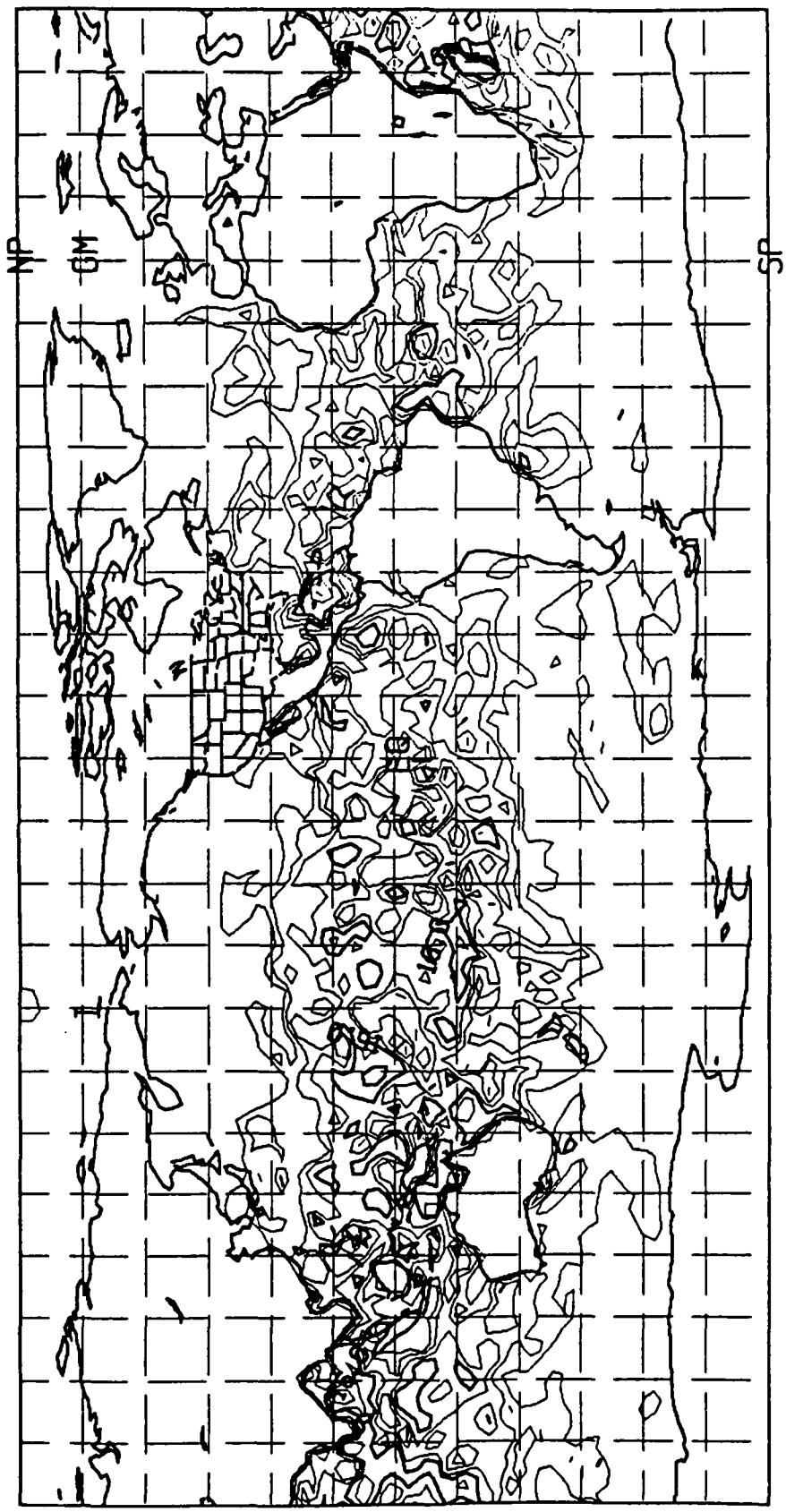

Figure 16. 36 hour forecast of the radar evaporative duct height field valid at 00Z on 26 June 1986.

throughout the period and agree well with the analysis, although the shape and exact location are more variable. Figure 13 shows an intense storm due south of Peru. The duct area off the coast of Peru appears to be coincident with the area of maximum winds. Note also the storms south of Australia and in the south Atlantic ocean in Figure 13. Figures 12 and 14-16 show that, while there is ducting south of Australia, the south Atlantic is duct-free throughout the period.

3.3 Tropics and Subtropics

The response of the SED product in the tropics and subtropics is typified by few forecasts of ducting in the central Indian ocean, central equatorial Pacific, and west equatorial Atlantic with somewhat better performance in the eastern Indian ocean and near the Asian continent. There is no significant diurnal difference.

In general, the ducting situation in the model is quite persistent with certain geographical areas favored for SED formation and certain other areas in which ducts rarely form. With the exception of the equatorial Pacific, all of the favored areas are near continents - east of Australia and Africa and in the South China Sea and Bay of Bengal. In the equatorial Pacific, there is a bias toward more extensive duct-filled areas for longer forecast periods. The persistence of the ducting situation in the tropics is not surprising; the weather in the tropics is also quite persistent. It is important to note that

there is almost no ducting activity forecast or analyzed in any of these summer cases off the coast of California, which is also an area favored for SED formation.

Some examples of the features discussed above from the summer of 1986 appear in Figures 12-21. In comparing Figures 14-16 (successive forecasts) with Figure 12 (the analysis from 00Z 26 June 1986), several important features are evident. For example, the extensive region of duct heights greater than 16 m extending across the Indian ocean and surrounding Australia in the analysis is present in the 12 hour forecast, present only east of Australia in the 24 hour forecast, and completely absent in the 36 hour forecast. Although forecast duct heights greater than 16 m are present in the central equatorial Pacific throughout the period, the exact location is quite variable. Some features which are better forecast are the area off the east coast of Africa from about 5 degrees S to about 25 degrees S and the area in the South China Sea and Bay of Bengal. The area of ducting in the equatorial Atlantic off the coast of Brazil appears consistently in all forecasts but is not realized; i.e., it is not in the analysis.

Many of the same features are present in a series of forecast valid at 12Z on 24 June 1986 (not shown) and in a similar series for 12Z on 30 June 1986 (Figures 17-21). In the 30 June series, ducting across the Indian ocean is not present although the area of ducting off the east coast of Africa is. Ducting east of Australia is also present. Ducting in the

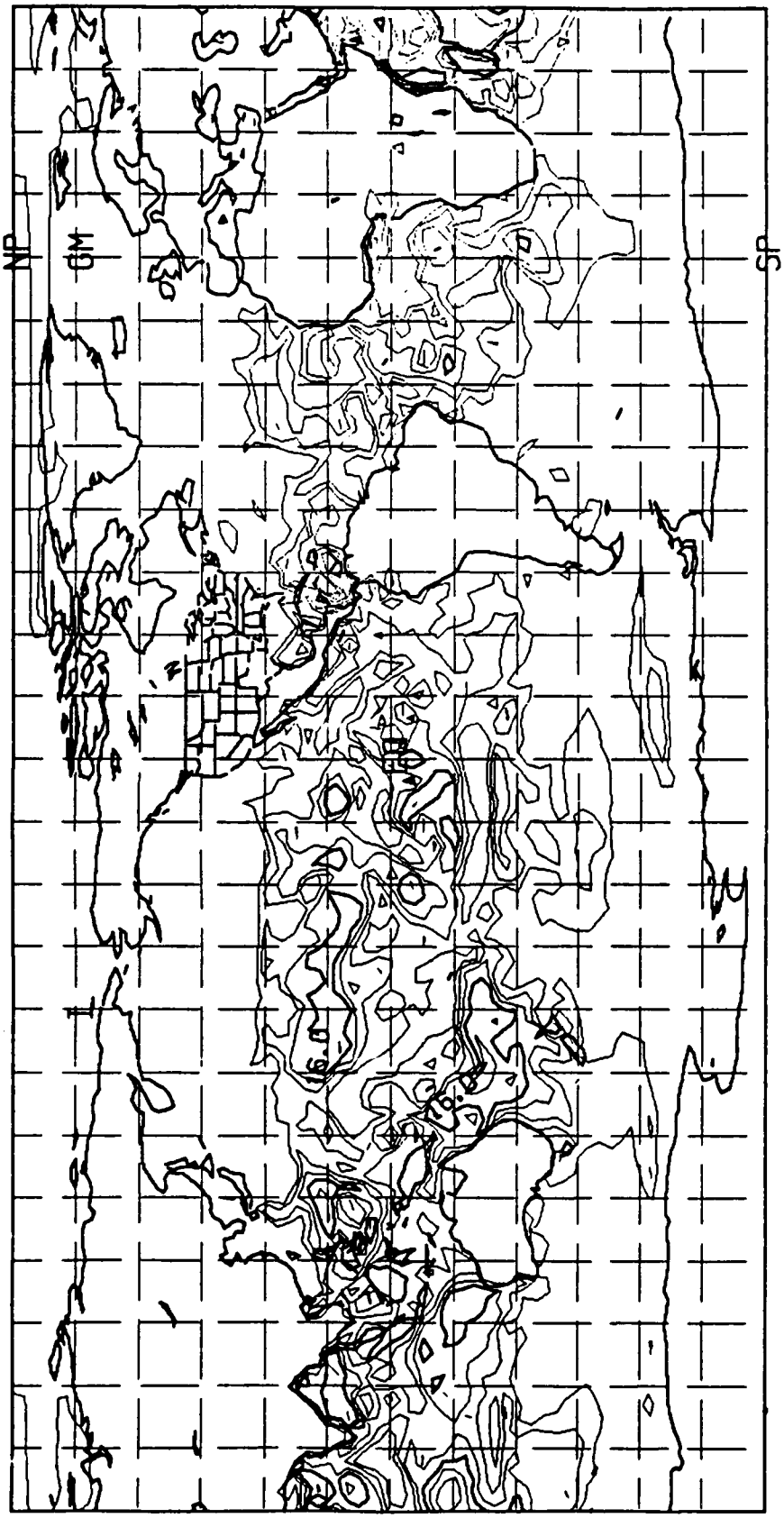

Figure 17. Analysis of the radar evaporative duct height field valid at 12Z on 30 June 1986.

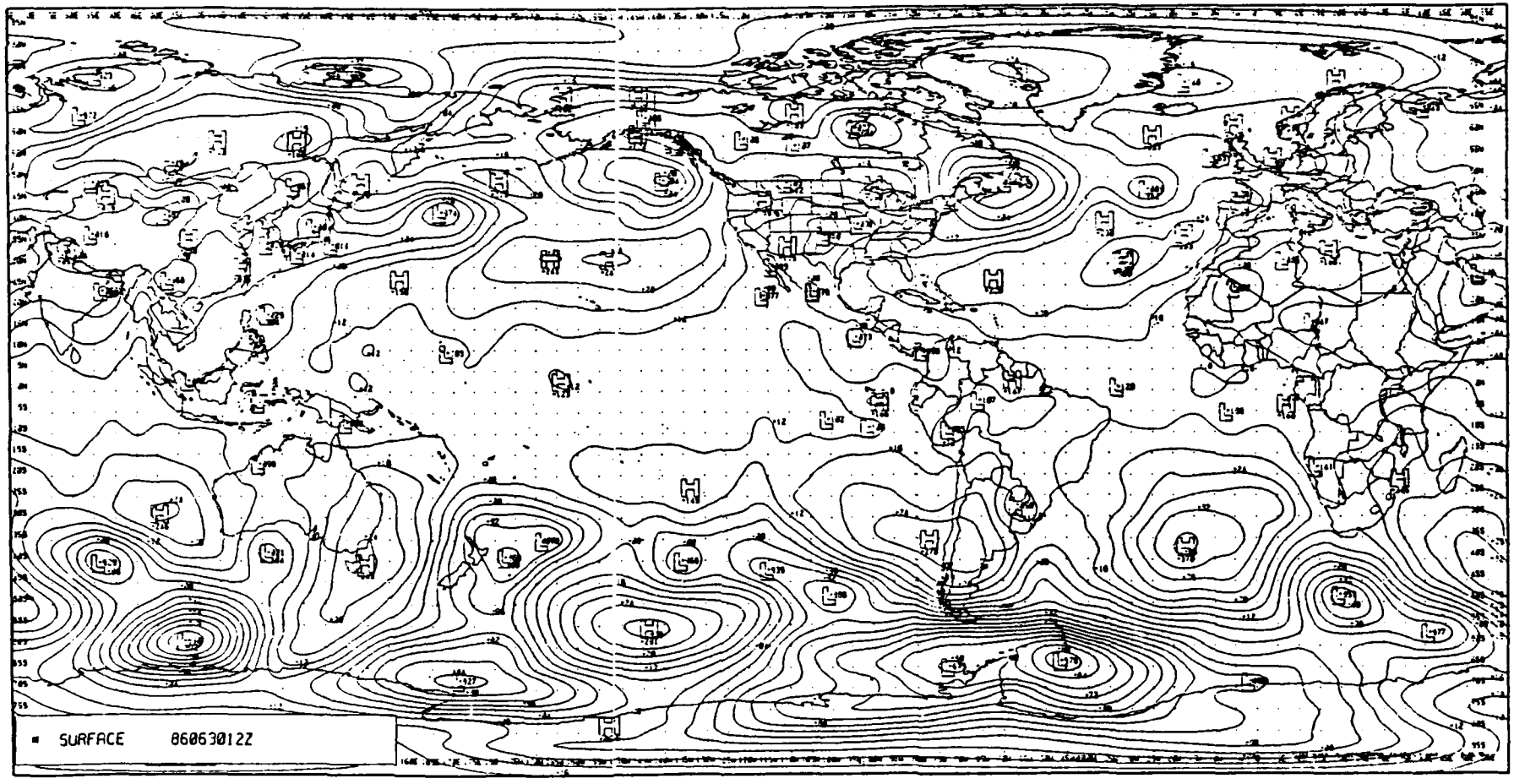

Figure 18. Analysis of the sea level pressure field valid at 12Z on 30 June 1986.

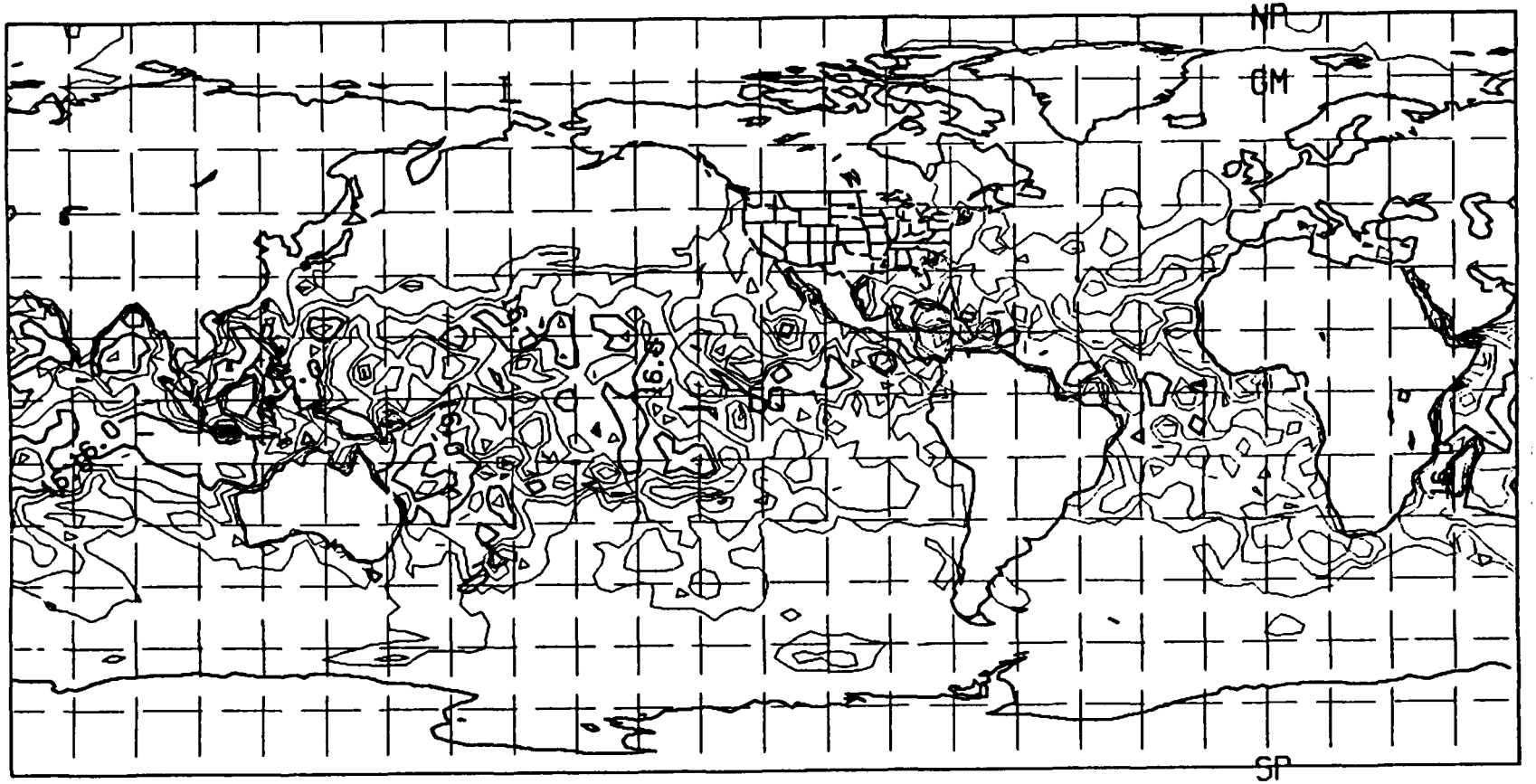

Figure 19. 12 hour forecast of the radar evaporative duct height field valid at 12Z on 30 June 1986.

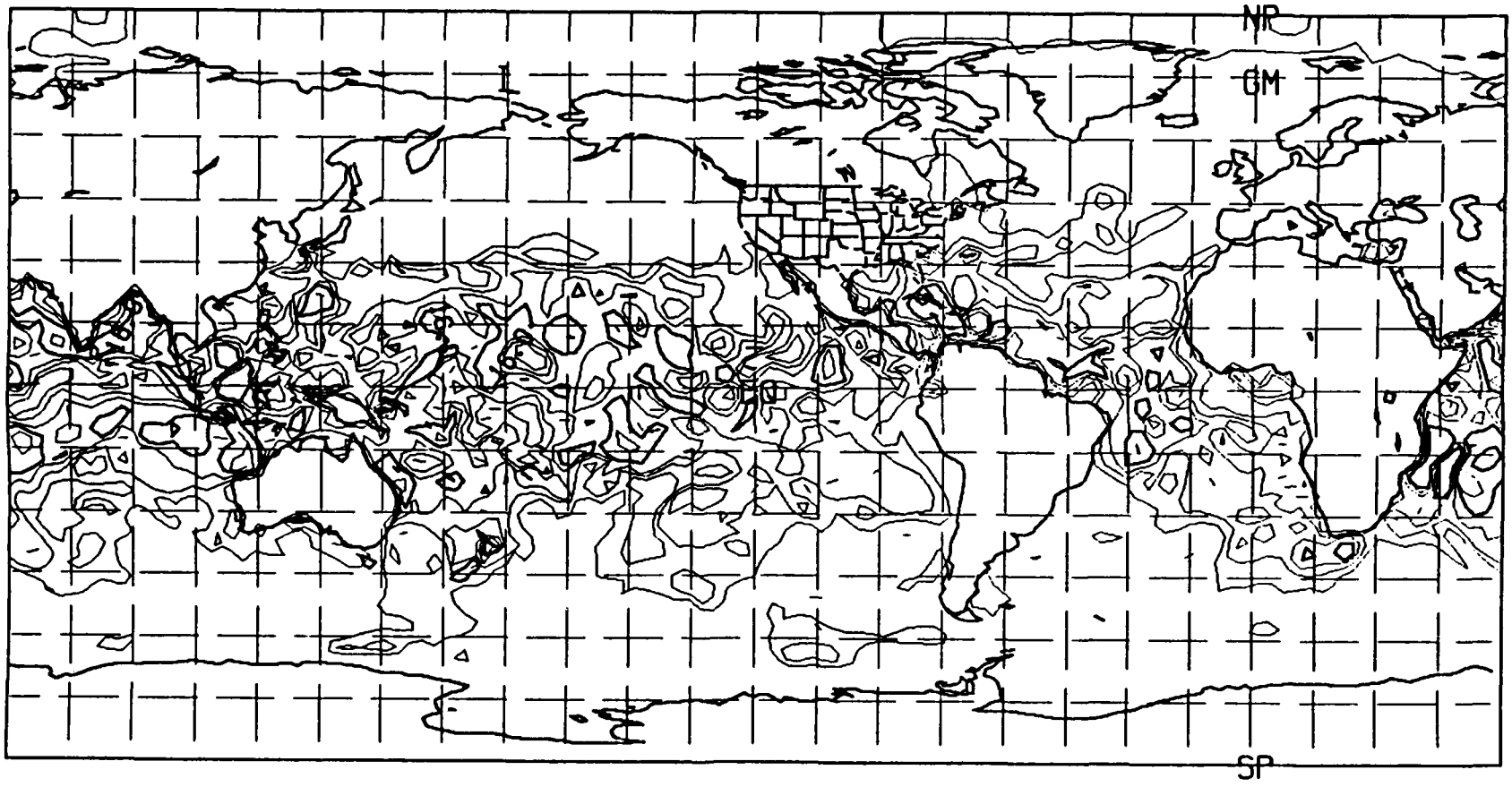

Figure 20. 24 hour forecast of the radar evaporative duct height field valid at 12Z on 30 June 1986.

Figure 21. 36 hour forecast of the radar evaporative duct height field valid at 12Z on 30 June 1986.

central equatorial Pacific is somewhat more extensive than in the 26 June series in both the analysis and the forecasts through 24 hours (at hour 36, the area is not as extensive as in the 26 June series). Also, the area extends further to the north (north of 15 degrees N). The ducting area in the South China Sea is not as apparent in the analysis, however, the area in the Bay of Bengal is present in the 30 June series. Even the nonrealizable feature in the equatorial Atlantic is present in this series.

4. CONCLUSION AND RECOMMENDATIONS

Surface evaporative ducts have considerable tactical significance in terms of the threat of detection by hostile units due to extended range, loss of the ability to detect hostile aircraft due to "holes", and danger of enhanced clutter. The only routinely available forecast aid for SED prediction is the SED product from the global surface contact layer interface model. The GSCLI model is a generalized similarity theory model for the entire PBL in which the NOGAPS low level pressure gradient, sea surface temperature, and 850 mb temperature are used. The method of stability determination, constraints placed on important parameters, and "engineering fixes" employed in the GSCLI warrant an examination of the quality of the SED product.

This evaluation of the SED product indicates that there is a considerable geographical bias in the quality of the SED forecasts. In the midlatitudes, the North Atlantic and South Pacific regions are well supported by the SED product while, in the North Pacific and South Atlantic, evaporative ducting is rarely forecast, regardless of the synoptic situation. In the

tropics and subtropics, persistent ducting conditions near continents are well forecast (except near Brazil, where forecast ducting almost never materializes) while ducting over open equatorial waters is poorly forecast.

It should be noted that, since the GSCLI is a purely diagnostic system, some of the apparent deficiencies in forecast fields may be reflections of deficiencies in the NOGAPS forecast fields used by the GSCLI. There is very little data in the tropics and most of it covers tropical continental areas. In the midlatitudes, extensive analyses of NOGAPS forecast fields performed at the FNOC have shown a consistent cold bias in near-surface air temperatures in the North Pacific ocean at all forecast times to 72 hours (Quality Control Division, 1986). This may play a role in the geographical bias of the A90 field in the North Pacific. No analyses have been performed on the Southern Hemisphere fields, but it is conceivable that similar behavior may be responsible for A90 performance in the South Atlantic.

It should also be noted that, since these analyses of the surface duct height product were completed, a new global analysis and forecast system (NOGAPS 3.0) has become operational at the FLENUMOCEANCEN. Therefore, some of the conclusions discussed herein regarding geographic variability may no longer be valid. An analysis similar to this one could be performed in order to assess the impact of NOGAPS 3.0 on the surface evaporative duct height product.

Based on the arguments presented in Appendices A and B, it is apparent that the expression used in the GSCLI model for the surface evaporative duct height possesses a serious shortcoming. When the ambient conditions are such that dN/dz never approaches the critical value, the GSCLI expression falsely produces reasonable appearing duct heights. This seems to be undesirable. It is recommended, therefore, that the similarity theory approach for potential refractivity presented in Appendix B be adopted under stable conditions for the operational surface evaporative duct height product.

REFERENCES

Businger, J., 1973: Turbulent transfer in the atmospheric surface layer. Workshop on Micrometeorology, D. Haugen, ed.. American Meteorological Society, Boston, MA. 392 pp.

Fleet Numerical Oceanography Center, 1986: Numerical Environmental Products Catalog, Vol. II. Commander, Naval Oceanography Command, NSTL, MS.

Ko, H. W., J. W. Sari, and J. P. Skura, 1983: Anomalous microwave propagation through atmospheric ducts. Johns Hopkins APL Technical Digest, 4, pg 12.

Paulus, R. A. and H. V. Hitney, 1979: Surface duct effects on radar/ESM detection range. Proceedings, Conference on Refractive Effects Assessment, 23-25 January 1979, San Diego, CA.

Quality Control Division, Code 443, 1986: Quarterly performance summary: September-November 1986. Fleet Numerical Oceanography Center, Monterey, CA. 64 pp.

Richter, J. H. and H. V. Hitney, 1979: The effects of atmospheric refractivity on microwave propagation. Proceedings, International Workshop on Atmospheric Water Vapor, 11-13 September 1979, Vail, CO.

Rosenthal, J., 1976: Refractive effects Guidebook (REG). Naval Environmental Prediction Research Facility, Monterey, CA.

Sketchly, J. F., 1979: Maritime surface ducting: UK measurement and theory. Proceedings, Conference on Refractive Effects Assessment, 23-25 January 1979, San Diego, CA.

Snyder, F. P., 1979: Radar clutter under atmospheric ducting conditions. Proceedings, Conference on Refractive Effects Assessment, 23-25 January 1979, San Diego, CA.

APPENDIX A

DERIVATION OF SURFACE EVAPORATIVE DUCT HEIGHT

The expression for δ in the GSCLI model can be obtained by taking the vertical derivative of the equation defining the index of refraction N:

$$N = APT^{-1} + APq(B/\epsilon)T^{-2} \tag{1}$$

$$\frac{dN}{dz} = \frac{\partial N}{\partial T}\frac{dT}{dz} + \frac{\partial N}{\partial q}\frac{dq}{dz} + \frac{\partial N}{\partial P}\frac{dP}{dz} \tag{2}$$

Evaluating the partial derivatives in (2) gives

$$\frac{\partial N}{\partial T} = -APT^{-2} - 2APq(B/\epsilon)T^{-3}$$

$$= -\frac{AP}{T^2}[1 + 2q(B/\epsilon T)] \tag{3}$$

$$\frac{\partial N}{\partial q} = \frac{AP}{T^2}(B/\epsilon) \tag{4}$$

$$\frac{\partial N}{\partial P} = \frac{A}{T} + \frac{AqB}{\epsilon T^2}$$

$$= \frac{A}{T}[1 + q(B/\epsilon T)]$$

but

$$dP/dz = -\rho g = -Pg/RT$$

thus,

$$\frac{\partial N}{\partial P}\frac{dP}{dz} = -\frac{AP}{T^2}[1 + q(B/\epsilon T)](g/R) \tag{5}$$

Using (3), (4), and (5), we can re-write (2) as

$$\frac{dN}{dz} = -\frac{AP}{T^2}\left[(1 + 2q(B/\epsilon T))\frac{dT}{dz} - (B/\epsilon)\frac{dq}{dz}\right.$$

$$\left. + (1 + q(B/\epsilon T))g/R\right] \qquad (6)$$

The remaining substantial derivatives in (6) can be evaluated from surface boundary layer similarity expressions:

$$\frac{dT}{dz} = \frac{T_*}{Kz}\phi(z/L) \qquad (7)$$

$$\frac{dq}{dz} = \frac{q_*}{Kz}\phi(z/L) \qquad (8)$$

Substituting (7) and (8) into (6) gives

$$\frac{dN}{dz} = -\frac{AP}{T^2}\left[\{(1 + 2q(B/\epsilon T))T_* - (B/\epsilon)q_*\}\frac{\phi(z/L)}{Kz}\right.$$

$$\left. + (1 + q(B/\epsilon T))g/R\right] \qquad (9)$$

At the duct height δ, the gradient in N is equal to the critical value b_2:

$$b_2 = -\frac{AP}{T^2}\left[\{(1 + 2q(B/\epsilon T))T_* - (B/\epsilon)q_*\}\frac{\phi(\delta/L)}{K\delta}\right.$$

$$\left. + (1 + q(B/\epsilon T))g/R\right] \qquad (10)$$

At this point, two simplifications are made in the derivation. First, in the stability function $\phi(\delta/L)$, δ is replaced by Z, a reference level. Retaining δ in $\phi(\delta/L)$ under unstable

conditions would require an iterative solution. Second, terms of order $qB/\epsilon T$ were neglected - this is difficult to justify; for a specific humidity of 10 g/Kg and an air temperature of 300 K, $qB/\epsilon T = 0.26$, $2qB/\epsilon T = 0.52$ which is certainly not small in comparison to 1 and, in the tropics, $2qB/\epsilon T$ may be ~O(1). We will proceed with the derivation of δ and then derive an alternate expression in which neither of the above simplifications are made. With the above simplifications, equation (10) becomes

$$b_2 = -\frac{AP}{T^2}\left[\{T_* - (B/\epsilon)q_*\}\frac{\phi(Z/L)}{K\delta} + g/R\right] \tag{11}$$

$$K\delta b_2 \frac{T^2}{AP} + g/R\ K\delta = (B/\epsilon)q_*\ \phi(Z/L) - T_*\ \phi(Z/L)$$

$$\delta = \frac{(B/\epsilon)q_*\ \phi(Z/L) - T_*\ \phi(Z/L)}{K((b_2T^2/AP) + g/R)} \tag{12}$$

Equation (12) is the expression used in the GSCLI model. Returning now to the full expression (10), we can derive an alternate expression for δ:

$$\delta = \frac{-\left[\{(1 + 2q(B/\epsilon T))T_* - (B/\epsilon)q_*\}\ \phi(\delta/L)\right]}{K[(b_2T^2/AP) - (1 + q(B/\epsilon T))g/R]} \tag{13}$$

Under stable conditions,

$$\phi(z/L) = 0.74 + 4.7(z/L) \tag{14}$$

Substituting (14) into (13) gives

$$\delta = \frac{-\left[\{(1 + 2q(B/\in T))T_* - (B/\in)q_*\}(\emptyset.74 + 4.7(\delta/L))\right]}{D}$$

where D is the denominator of (13); i.e.,

$$D = K[(b_2 T^2/AP) - (1 + q(B/\in T))g/R]$$

$$\delta = -[\emptyset.74\{(1 + 2q(B/\in T))T_* - (B/\in)q_*\} + 4.7(\delta/L)\{(1 + 2q(B/\in T))T_* - (B/\in)q_*\}]\ D^{-1}$$

$$\delta = \frac{-\emptyset.74\{(1 + 2q(B/\in T))T_* - (B/\in)q_*\}}{D + 4.7/L\{1 + 2q(B/\in T))T_* - (B/\in)q_*} \qquad (15)$$

Under unstable conditions,

$$\phi(z/L) = \emptyset.74(1 - 9(z/L))^{-1/2} \qquad (16)$$

Substituting (16) into (13) gives

$$\delta = -[\{(1 + 2q(B/\in T))T_* - (B/\in)q_*\} \times (\emptyset.74(1 - 9(\delta/L))^{-1/2}]\ D^{-1}$$

$$\delta(1 - 9(\delta/L))^{-1/2} = -\emptyset.74[(1 + 2q(B/\in T))T_* - (B/\in)q_*]\ D^{-1} \qquad (17)$$

Equations (15) and (17) are considerably more complicated than (12). In order to assess the significance of the differences between (12) and (15) and (17), a program was written which evaluates (12) and either (15) or (17), depending on atmospheric

stability. Results produced by the program revealed that, in near-neutral conditions, the two expressions produced very nearly identical results. For increasing stability, the full expression (15) gave duct heights substantially larger than the expression (12) used in the GSCLI model. Under unstable conditions, the Newton-Raphson technique was used to solve (17). Solutions were obtained in 3-5 iterations with an initial estimate of 10 m. Equations (17) and (12) produced similar results. Results also revealed an important characteristic of equation (12). An assumption inherent in (10) is that, somewhere in the surface layer, $dN/dz = b_2$;i.e., that a surface evaporative duct exists. When this is not the case, (12) still produces values that appear to be resonable for duct height. In reality, when $dN/dz << [b_2]$, no duct exists and when $dN/dz >> [b_2]$, the surface evaporative duct height is greater than the depth of the surface layer and there is strong trapping extending up the elevation at which $dN/dz < [b_2]$. Equations (15) and (17) produce very shallow duct heights when $dN/dz >> [b_2]$ and large negative duct heights when $dN/dz << [b_2]$. The fact that equation (12) produces false indications of reasonable duct thickness in these situations seems undesirable.

APPENDIX B

APPLICATION OF SURFACE SIMILARITY THEORY TO POTENTIAL REFRACTIVITY

In this Appendix we first demonstrate that potential refractivity can be scaled by the same type of surface layer similarity expressions as commonly used for temperature and moisture (ordinary refractivity cannot be treated this way, however). Then, using this similarity expression for potential refractivity, we derive expressions for evaporative duct height as a function of stability. This method of computing duct height is then commpared with others discussed in this report.

Similarity theory as applied to mean and turbulence variables shows that many parameters follow simple scaling laws in the atmosheric surface layer. The functional forms of these scaling laws have been fairly well established by observational studies. For example, in the surface layer, nondimensional temperature and moisture gradients follow the scaling laws:

$$\frac{\kappa z}{T_*}\frac{\partial T}{\partial z} = \phi_h (Z/L) , \qquad (1)$$

$$\frac{\kappa z}{q_*}\frac{\partial q}{\partial z} = \phi_q (Z/L) , \qquad (2)$$

where T_* and q_* are scaling parameters and L is the Monin-Obukhov length. Generally the universal functions for heat and moisture are taken to be equal, i.e., $\phi_h = \phi_q = \phi$.

It is often assumed (without proof) that refractivity can be scaled in the same manner, so that

$$\frac{\kappa z}{N_\star}\frac{\partial N}{\partial z} = \phi(Z/L) \ , \tag{3}$$

but we will see that this is wrong. The expression for refractivity in the microwave region of the spectrum is

$$N = \frac{A}{T}\left[P + \frac{BPq}{\varepsilon T}\right]. \tag{4}$$

A quantity called potential refractivity, χ, can be defined such that it does not vary with pressure:

$$\chi = \frac{A}{T}\left[P_o + \frac{BP_oq}{\varepsilon T}\right] \tag{5}$$

where P_o = 1000 mb. A total differential of χ is

$$d\chi = \frac{\partial \chi}{\partial T}\,dT + \frac{\partial \chi}{\partial q}\,dq \ . \tag{6}$$

Replacing the differentials in (6) with fluctuation notation (a common trick in turbulence derivations) yields:

$$\chi' = \frac{\partial \chi}{\partial_T}\,T' + \frac{\partial \chi}{\partial_q}\,q' \ . \tag{7}$$

If we multiply (7) by -w' divide by $U_\star$, and average:

$$-\frac{\overline{w'\chi'}}{U_\star} = \left(\frac{\partial \chi}{\partial T}\right)\left(-\frac{\overline{w'T'}}{U_\star}\right) + \left(\frac{\partial \chi}{\partial q}\right)\left(-\frac{\overline{w'q'}}{U_\star}\right) \tag{8}$$

or, using the standard notation of scaling parameters,

$$\chi_* = \frac{\partial \chi}{\partial T} T_* + \frac{\partial \chi}{\partial q} q_* \ . \tag{9}$$

Returning now to (6) and writing χ as a total vertical derivative,

$$\frac{d\chi}{dz} = \frac{\partial \chi}{\partial T} \frac{dT}{dz} + \frac{\partial \chi}{\partial q} \frac{dq}{dz} \ , \tag{10}$$

and substituting (1) and (2) for the temperature and moisture gradients gives:

$$\frac{d\chi}{dz} = \left[\left(\frac{\partial \chi}{\partial T}\right) T_* + \left(\frac{\partial \chi}{\partial q}\right) q_* \right] \frac{\phi(z/L)}{kz} \ . \tag{11}$$

Now, using (9) we can rewrite (11) as:

$$\frac{d\chi}{dz} = \chi_* \frac{\phi(z/L)}{\kappa z}$$

or,

$$\frac{\kappa z}{\chi_*} \frac{d\chi}{dz} = \phi(z/L) \ . \tag{12}$$

Thus, we have proved that the potential refractivity obeys surface layer similarity.

Note, however, that had we attempted this derivation with N rather than χ, we would have found in place of (8):

$$-\frac{\overline{w'N'}}{u_*} = \left(\frac{\partial N}{\partial T}\right)\left(-\frac{\overline{w'T'}}{u_*}\right) + \left(\frac{\partial N}{\partial q}\right)\left(-\frac{\overline{w'q'}}{u_*}\right) + \left(\frac{\partial N}{\partial p}\right)\left(-\frac{\overline{w'p'}}{u_*}\right) \tag{13}$$

and we could not have easily treated the last term in this expression. Thus, it is proper to treat $\chi(T,q)$ as a similarity variable, but not $N(T,q,p)$.

We know that the critical refractivity gradient for trapping,

$$\left(\frac{dN}{dz}\right)_c,$$

is $-0.157\ m^{-1}$. Now we need to know what this corresponds to in terms of

$$\frac{d\chi}{dz}.$$

First, by examination of (4) and (5) we note that

$$\frac{\partial N}{\partial T} = \frac{\partial \chi}{\partial T} \quad \text{and} \quad \frac{\partial N}{\partial q} = \frac{\partial \chi}{\partial q} \tag{14}$$

Taking a total derivative of (4) gives

$$\frac{dN}{dz} = \frac{\partial N}{\partial T}\frac{dT}{dz} + \frac{\partial N}{\partial q}\frac{dq}{dz} + \frac{\partial N}{\partial p}\frac{dp}{dz} \tag{15a}$$

or,

$$\frac{dN}{dz} = \frac{\partial \chi}{\partial T}\frac{dT}{dz} + \frac{\partial \chi}{\partial q}\frac{dq}{dz} + \frac{\partial N}{\partial p}\frac{dp}{dz} \tag{15b}$$

so that,

$$\frac{dN}{dz} = \frac{d\chi}{dz} + \frac{\partial N}{\partial p}\frac{dp}{dz}. \tag{16}$$

Thus,
$$\left(\frac{d\chi}{dz}\right)_c = \left(\frac{dN}{dz}\right)_c - \frac{\partial N}{\partial p}\frac{dp}{dz}. \tag{17}$$

Using the hydrostatic equation, $\frac{dp}{dz} = -\frac{pg}{R_d T}$, gives[1]

$$\left(\frac{d\chi}{dz}\right)_c = \left(\frac{dN}{dz}\right)_c + \frac{pg}{R_d T}\frac{\partial N}{\partial p} \quad . \tag{18}$$

From (4) we find

$$\frac{\partial N}{\partial p} = \frac{A}{T}\left[1 + \frac{Bq}{\varepsilon T}\right] , \tag{19}$$

so that,

$$\left(\frac{d\chi}{dz}\right)_c = \left(\frac{dN}{dz}\right)_c + \frac{pgA}{R_d T^2}\left[1 + \frac{Bq}{\varepsilon T}\right] . \tag{20}$$

Thus, the critical χ gradient is not a constant, but rather a function of p, T, and q. We can estimate a typical magnitude of this last term by selecting p = 1000 mb, T = 300°k, and q = 10^{-2}. Then

$$pg\frac{A}{R_d T^2}\left[1 + \frac{Bg}{T}\right] \simeq 0.037.$$

Thus,

$$\left(\frac{d\chi}{dz}\right)_c = -0.157 + 0.037 = -0.120 \text{ m}^{-1} .$$

The IREPS model uses a constant value of -0.125 m^{-1} for the critical gradient of refractivity.

---

[1] We purposely have not written the hydrostatic equation in terms of density because the coefficients A and B are dimensional and the values we are using are designed to be used in conjunction with pressure in ... .

If we let $\gamma = \left(\frac{d\chi}{dz}\right)_c$, and treat this as a constant, we may write (12) as:

$$\frac{\kappa\delta}{\chi_*}(\gamma) = \phi\left(\frac{\delta}{L}\right) \tag{21}$$

where δ is the duct height at which χ reaches its critical gradient. For $\phi(z/L)$ we take [Businger, 1973]

$$\phi(Z/L) = \begin{cases} .74 + 4.7(z/L) & L \geq \text{ (neutral, stable)} \\ .74(1 - 9\ z/L)^{-1/2} & L < 0 \quad \text{(unstable} \end{cases} \tag{22}$$

Substituting (22) into (21) we find, for <u>stable</u> conditions:

$$\delta = .74\left(\frac{\kappa\gamma}{\chi_*} - \frac{4.7}{L}\right)^{-1} = \frac{.74\chi_*}{\kappa\gamma}\left(1 - \frac{4.7\chi_*}{\kappa\gamma_L}\right)^{-1} \tag{23}$$

[At this point we only note in passing that the expression for δ can go negative under certain conditions.]

For <u>unstable</u> conditions we find,

$$\delta\left(1 - 9\frac{\delta}{L}\right)^{1/2} = \frac{.74\chi_*}{\kappa\gamma} \tag{24}$$

For ease of use with a Newton-Raphson technique, we square this equation and rearrange as:

$$F(\delta) = \delta^2\left(1 - 9\frac{\delta}{L}\right) - \left(\frac{.74\chi_*}{\kappa\gamma}\right)^2 = 0 \tag{25}$$

The derivative of this equation is

$$F'(\delta) = 2\delta - 3\left(\frac{9\delta^2}{L}\right) \tag{26}$$

and thus we can solve for δ by the Newton-Raphson iterative method:

$$\delta^{(m+1)} = \delta^{(m)} - \frac{F(\delta^{(m)})}{F'(\delta^{(m)})} \tag{27}$$

where $\delta^{(m+1)}$ is the (m+1) approximation to δ. This converges rapidly. Thus, we can solve for duct height by use of either (23) or (24) provided we have χ_*. And χ_* can be found by first noting (analogous to T and q) we can write the integrated form of (12) as

$$\chi(z) - \chi(z_o) = \frac{.74\chi_*}{\kappa} [\ln z/z_o - \psi(z/L)] \tag{28}$$

or, rewriting as,

$$\chi_* = \frac{\kappa[\chi(z) - \chi(z_o)]}{.74[\ln z/z_o - \psi(z/L)} \quad . \tag{29}$$

Here $\psi(z/L)$ are integrated forms of $\phi(z/L)$ and have been found to be

$$\psi(z/L) = \begin{cases} -\frac{4.7}{.74} z/L & , L \geq 0 \\ 2 \ln \frac{(1+y)}{2} & , L < 0 \end{cases} \tag{30}$$

where, $y = (1-9Z/L)^{1/2}$.

Now we summarize the steps for computing the evaporation duct height δ based on a similarity expression for potential refractivity, χ. We assume that we already know values of T and q at some reference height, z_r, and we know the sea surface

temperature. Further, we assume that we have already computed L and z_o from expressions that we do not discuss here.

1. Compute $\chi(z_r)$ and $\chi(z_o)$ using (5).
2. Compute χ_* from (29) with $z \to z_r$.
3. Depending on the sign of L, compute δ either from (23) or (24).

Of the different methods discussed in this report for finding δ, the method outlined above appears to be the most accurate and to require relatively little computing power.

Distribution of this report:

Fleet Numerical Oceanography Center

Defense Technical Information Center